Author Manuscript Published OnlineFirst on May 12, 2021; DOI: 10.1158/0008-5472.CAN-20-2496
Author manuscripts have been peer reviewed and accepted for publication but have not yet been edited.

Cancer-associated fibroblasts in pancreatic ductal adenocarcinoma determine response to SLC7A11 inhibition

Authors: George Sharbeen[1†], Joshua A. McCarroll[2,3,4†], Anouschka Akerman[1†], Chantal Kopecky[1], Janet Youkhana[1], John Kokkinos[1,3], Jeff Holst[5], Cyrille Boyer[3], Mert Erkan[6], David Goldstein[1,7], Paul Timpson[8,9,10], Thomas R. Cox[8,9,10], Brooke A. Pereira[8,9,10], Jessica L. Chitty[8,10], Sigrid K. Fey[11], Arafath K. Najumudeen[11], Andrew D. Campbell[11], Owen J. Sansom[11], Rosa Mistica C. Ignacio[1], Stephanie Naim[1], Jie Liu[1], Nelson Russia[1], Julia Lee[1], Angela Chou[8,12], Amber Johns[9], Anthony J. Gill[8,9,13], Estrella Gonzales-Aloy[1], Val Gebski[14], Yi Fang Guan[5], Marina Pajic[8,9], Nigel Turner[15], Minoti V. Apte[16], Thomas P. Davis[17], Jennifer P. Morton[18], Koroush S. Haghighi[7], Jorjina Kasparian[1], Benjamin J. McLean[8], Yordanos F. Setargew[8], Australian Pancreatic Cancer Genome Initiative[9], Phoebe A. Phillips[1,3*].

Affiliations:

[1]*Pancreatic Cancer Translational Research Group, Prince of Wales Clinical School and School of Medical Sciences, Lowy Cancer Research Centre, UNSW Sydney, NSW, Australia*

[2]*Children's Cancer Institute, Lowy Cancer Research Centre, UNSW Sydney, NSW, Australia*

[3]*Australian Centre for Nanomedicine, ARC Centre of Excellence in Convergent Bio-Nano Science and Technology, UNSW Sydney, NSW, Australia*

[4]*School of Women's and Children's Health, UNSW Sydney, NSW, Australia*

[5]*School of Medical Science and Prince of Wales Clinical School, Lowy Cancer Research Centre, UNSW Sydney, Sydney, NSW, Australia*

[6]*Koc University Research Centre for Translational Medicine and Department of Surgery, Koc University, School of Medicine, Istanbul, Turkey*

[7]*Prince of Wales Hospital, Prince of Wales Clinical School, Sydney, NSW, Australia*

[8]*The Garvan Institute of Medical Research and the Kinghorn Cancer Centre, Sydney, NSW, Australia*

[9]*Australian Pancreatic Cancer Genome Initiative (APGI), Sydney, NSW, Australia*

[10]*St. Vincent's Clinical School, UNSW Sydney, Sydney, NSW, Australia*

[11]*Cancer Research UK, Beatson Institute, Glasgow, United Kingdom*

[12]*Department of Anatomical Pathology, Royal North Shore Hospital, University of Sydney, Sydney, NSW, Australia*

Downloaded from cancerres.aacrjournals.org on July 31, 2021. © 2021 American Association for Cancer Research.

Author Manuscript Published OnlineFirst on May 12, 2021; DOI: 10.1158/0008-5472.CAN-20-2496
Author manuscripts have been peer reviewed and accepted for publication but have not yet been edited.

[13]*Cancer Diagnosis and Pathology Group, Kolling Institute of Medical Research, Royal North Shore Hospital, University of Sydney, Sydney, NSW, Australia*

[14]*NHMRC Clinical Trials Centre, University of Sydney, NSW, Australia*

[15]*School of Medical Sciences, UNSW Sydney, NSW, Australia*

[16]*Pancreatic Research Group, South Western Sydney Clinical School, UNSW and Ingham Institute for Applied Medical Research, Sydney, Australia*

[17]*ARC Centre of Excellence in Convergent Bio-Nano Science and Technology, Monash Institute of Pharmaceutical Sciences, Monash University, Australia*

[18]*Institute of Cancer Sciences, University of Glasgow, Glasgow UK*. * Corresponding author. †Share first author position.

Running title: SLC7A11 inhibition reprograms pancreatic cancer stroma.

Keywords: Pancreatic cancer-associated fibroblasts, SLC7A11, pancreatic cancer, stromal remodelling, nanoparticles.

Corresponding author: A/Prof Phoebe Phillips. Address: Head, Pancreatic Cancer Translational Research Group, Adult Cancer Program, Lowy Cancer Research Centre, UNSW Sydney, NSW, Australia, 2052. Phone: +612-9385-3299. Email: p.phillips@unsw.edu.au

Conflicts of interest. The authors declare no potential conflict of interest.

Downloaded from cancerres.aacrjournals.org on July 31, 2021. © 2021 American Association for Cancer Research.

Author Manuscript Published OnlineFirst on May 12, 2021; DOI: 10.1158/0008-5472.CAN-20-2496
Author manuscripts have been peer reviewed and accepted for publication but have not yet been edited.

ABSTRACT

Cancer-Associated Fibroblasts (CAF) are major contributors to pancreatic ductal adenocarcinoma (PDAC) progression through pro-tumor signalling and the generation of fibrosis, the latter of which creates a physical barrier to drugs. CAF inhibition is thus an ideal component of any therapeutic approach for PDAC. SLC7A11 is a cystine transporter that has been identified as a potential therapeutic target in PDAC cells. However, no prior study has evaluated the role of SLC7A11 in PDAC tumor stroma and its prognostic significance. Here we show that high expression of SLC7A11 in human PDAC tumor stroma, but not tumor cells, is independently prognostic of poorer overall survival. Orthogonal approaches showed that PDAC-derived CAFs are highly dependent on SLC7A11 for cystine uptake and glutathione synthesis and that SLC7A11 inhibition significantly decreases CAF proliferation, reduces their resistance to oxidative stress, and inhibits their ability to remodel collagen and support PDAC cell growth. Importantly, specific ablation of SLC7A11 from the tumor compartment of transgenic mouse PDAC tumors did not affect tumor growth, suggesting the stroma can substantially influence PDAC tumor response to SLC7A11 inhibition. In a mouse orthotopic PDAC model utilizing human PDAC cells and CAFs, stable knockdown of SLC7A11 was required in both cell types to reduce tumor growth, metastatic spread, and intratumoral fibrosis, demonstrating the importance of targeting SLC7A11 in both compartments. Finally, treatment with a nanoparticle gene-silencing drug against SLC7A11, developed by our laboratory, reduced PDAC tumor growth, incidence of metastases, CAF activation, and fibrosis in orthotopic PDAC tumors. Overall, these findings identify an important role of SLC7A11 in PDAC-derived CAFs in supporting tumor growth.

Statement of Significance: This study demonstrates that SLC7A11 in PDAC stromal cells is important for the tumor-promoting activity of CAF and validates a clinically translatable nanomedicine for therapeutic SLC7A11 inhibition in PDAC.

Downloaded from cancerres.aacrjournals.org on July 31, 2021. © 2021 American Association for Cancer Research.

Author Manuscript Published OnlineFirst on May 12, 2021; DOI: 10.1158/0008-5472.CAN-20-2496
Author manuscripts have been peer reviewed and accepted for publication but have not yet been edited.

INTRODUCTION

Pancreatic ductal adenocarcinoma (PDAC) is a lethal malignancy, with a 5-year survival rate of <9% (1). A major reason for this poor prognosis is the drug-refractory nature of PDAC caused by inherent chemoresistance and physical barriers to drug delivery. The dense fibrotic microenvironment drives these mechanisms (2-4). Fibrosis distorts the tumour vasculature physically hindering drug access and creates a harsh hypoxic and nutrient-deprived microenvironment, which promotes a more metastatic and chemoresistant mesenchymal phenotype (2-4). The architects of the PDAC microenvironment are Cancer-Associated Fibroblasts (CAFs) (2-4). CAFs are activated by signals released from PDAC cells and hypoxia, resulting in a self-perpetuating loop of excessive extracellular matrix (ECM) protein deposition that creates fibrosis (2-4). CAFs also reciprocate pro-survival signalling to PDAC cells, thus promoting PDAC cell survival and epithelial to mesenchymal transition (2-4). This makes stromal remodelling and inhibition of CAF activity an important consideration for PDAC therapies.

CAFs and PDAC cells share an oxygen/nutrient poor microenvironment. PDAC cells have altered their metabolism to survive and proliferate in this stressful microenvironment (5). These alterations lead to metabolic addictions that can be therapeutically exploited. A potential target is the X_c^- amino acid antiporter, which imports cystine into the cell, in exchange for glutamate (6-8). X_c^- is a heterodimer of solute carrier 3A2 (SLC3A2; membrane anchor) and solute carrier 7A11 (SLC7A11, also known as xCT; amino acid transporter) (6-8). This transporter sits at the crux of multiple metabolic activities necessary for cancer cell survival, including protein synthesis and redox regulation. First, cystine transported by SLC7A11 is reduced to cysteine, which is an irreplaceable component of proteins, that is required for disulphide bond formation. Second, cysteine is also the rate-limiting amino acid in the synthesis of the potent antioxidant glutathione (GSH) (9). GSH is important in PDAC cell survival as KRAS-driven metabolic changes, pro-tumour signalling and microenvironment-driven hypoxia increase otherwise lethal intracellular oxidative stress (10).

SLC7A11 has been identified as a prognostic factor and potential therapeutic target in a number of cancers (11-16). In PDAC, Lo et al (17) demonstrated that SLC7A11 was upregulated in

Downloaded from cancerres.aacrjournals.org on July 31, 2021. © 2021 American Association for Cancer Research.

Author Manuscript Published OnlineFirst on May 12, 2021; DOI: 10.1158/0008-5472.CAN-20-2496
Author manuscripts have been peer reviewed and accepted for publication but have not yet been edited.

PDAC cells under oxidative stress and cystine deprivation *in vitro*, and SLC7A11 inhibition (sulfasalazine,SSZ) significantly reduced subcutaneous PDAC tumour growth (18). Since then, studies have demonstrated the autophagic regulation (19) and therapeutic potential of inhibiting or genetically ablating SLC7A11 in PDAC cells (20-24). While promising, a key limitation of these studies was that they ignored the role of SLC7A11 in CAFs or the impact of CAFs on PDAC cell sensitivity to SLC7A11 inhibition. This is a critical gap in our knowledge for therapeutic inhibition of SLC7A11 in PDAC, given the prominent role CAFs play in PDAC cell survival and drug sensitivity and their potential to help overcome nutrient deficiencies (25,26).

We hypothesised that SLC7A11 inhibition in CAFs had the potential to directly inhibit a key cellular target in PDAC and to break pro-tumour interactions between CAFs and PDAC cells. We demonstrate that high stromal expression of SLC7A11 predicts poorer patient survival, and that SLC7A11 inhibition in CAFs reduces their proliferation, anti-oxidant capacity and growth of 3D spheroid co-cultures with PDAC cells. Importantly, we show that stable knockdown of SLC7A11 in CAFs reduces tumour incidence, growth and fibrosis, and demonstrate the therapeutic potential of inhibiting SLC7A11 expression in PDAC tumours using a gene silencing nanomedicine.

MATERIALS AND METHODS

Cell isolation and culture.

Commercial human PDAC cells (MiaPaCa-2, Panc-1, AsPC1, HPAFII; American Tissue Culture Collection) were cultured as described (27-29). The TKCC5 human pancreatic cancer cells were established from patient-derived xenografts (PDX) and cultured as described (30). PDAC cell purity was confirmed by short tandem-repeat profiling (CellBank Australia). Human Pancreatic Ductal Epithelial (HPDE) cells (a gift from Ming Tsao, Ontario Cancer Institute) were cultured as described (31). All studies involving the use of human-derived fibroblasts and CAFs were approved by the UNSW Sydney human ethics committee (approvals: HC14039, HC180973, HREC13/023) and the German Technical University of Munich human ethics committee (approval: 5510/12). All patients provided written informed consent. Quiescent human pancreatic fibroblasts, activated by culture on plastic, were isolated from patients with benign pancreatic conditions as described (32). Human CAFs were isolated from PDAC tumour tissue

Downloaded from cancerres.aacrjournals.org on July 31, 2021. © 2021 American Association for Cancer Research.

Author Manuscript Published OnlineFirst on May 12, 2021; DOI: 10.1158/0008-5472.CAN-20-2496
Author manuscripts have been peer reviewed and accepted for publication but have not yet been edited.

by explant culture and used within 12 passages as described (33,34). All CAFs were cultured in IMDM, 10% FBS, 4mM L-glutamine. The purity of CAFs was assessed by positive immunostaining for glial fibrillary acidic protein (GFAP) and alpha-smooth muscle actin (αSMA) and negative immunostaining for cytokeratin, as described (32). Cells were maintained in a humidified incubator (37°C, 5% CO_2) and tested negative for mycoplasma [MycoAlert Mycoplasma Detection kit (Lonza)] during fortnightly testing throughout study.

Immortalisation of human PDAC CAFs and establishment of human PDAC and CAF cells expressing SLC7A11 shRNA.

Human patient-derived CAFs (passage 9) were immortalised by lentiviral delivery of a human telomerase construct (GenTarget, Cat. LVP1131-RP). Cells were maintained in puromycin and red fluorescent protein positive cells sorted on a BD FACS Aria II. We confirmed hTERT-CAFs had comparable proliferation to parent cells. MiaPaCa-2 cells and hTERT-immortalised CAFs were then transduced with lentiviral scramble(control)-shRNA, SLC7A11-shRNA sequence 1 constructs (Origene, Cat. TL309282). Transduced cells were maintained in puromycin and GFP positive cells sorted on a BD FACS Melody. Western blot confirmed SLC7A11 knockdown. All CAF shRNA cell lines were re-validated as per patient-derived CAFs and used within 50 passages of immortalisation.

Isolation and culture of KPC transgenic mouse PDAC and CAF cells.

Mouse KPC PDAC cells were isolated from tumours from the KPC genetically engineered mouse model (KRAS/P53-mutated) and cultured as described (35). KPC CAFs were isolated as described (33,34) and validated by immunocytochemistry for GFAP and αSMA. KPC CAFs were cultured as per human CAFs (33,34).

Quantitative real-time PCR (qPCR).

qPCR was performed using Power SYBR® green kit (ThermoFisher Scientific) run on an Applied Biosystems ViiA7 platform. Primers were obtained from Qiagen: SLC7A11 (Cat. QT00002674); 18S ribosomal RNA (housekeeping gene, Cat. QT00199367); SLC3A2 (Cat. QT00085897); β_2-microglobulin (housekeeping gene, Cat. QT00199367). Concentrations were

Downloaded from cancerres.aacrjournals.org on July 31, 2021. © 2021 American Association for Cancer Research.

Author Manuscript Published OnlineFirst on May 12, 2021; DOI: 10.1158/0008-5472.CAN-20-2496
Author manuscripts have been peer reviewed and accepted for publication but have not yet been edited.

calculated based on ΔCt standard curves and standardised to β_2-microglobulin or 18S ribosomal RNA.

Western blot for SLC7A11.

Protein lysates were prepared, quantified, electrophoresed on a 10% SDS-PAGE gel and transferred to nitrocellulose membranes as described (27), except samples were not boiled before electrophoresis. Membranes were probed with primary and secondary antibodies detailed in **supplementary table 1**. Blots were visualised and bands quantified as described (27).

Validation of SLC7A11 antibodies.

Serial sections of formalin-fixed, paraffin-embedded human PDAC tumour tissue were obtained through the Australian Pancreatic Cancer Genome Initiative (APGI). All studies involving the use of human specimens were approved by the UNSW Sydney human ethics committee (approvals: HC14039, HC180973, HREC13/023). All patient provided written informed consent through the APGI. Antigen retrieval was performed as described (27-29). Tissue sections were probed with antibodies detailed in **supplementary table 1**, then Vectastain® ABC kit (Vector laboratories). 3,3' diaminobenzidine (DAB) was used as the substrate and hematoxylin as counter-stain. The Cell Signaling antibody used for this study was validated as detailed in (36). We showed similar staining patterns in PDAC tissue sections using 3 independent antibodies (**Figure S1A**). Positive control brain tissue (**Figure S1B**) showed abundant SLC7A11 staining and negative control skin tissue (**Figure S1B**) showed no SLC7A11 staining, consistent with expression in the human protein atlas. Specificity was also confirmed by its ability to detect specific SLC7A11 gene silencing (2 siRNAs and shRNA) in Western blot (**Figure S1C-F**).

Immunofluorescence for SLC7A11 and αSMA co-localisation.

Formalin-fixed, paraffin-embedded human PDAC tumour tissue was obtained through the APGI. Antigen retrieval was performed as described (27-29). Tissue sections were then stained with primary and secondary antibodies detailed in **supplementary table 1**. Tissues were mounted

Downloaded from cancerres.aacrjournals.org on July 31, 2021. © 2021 American Association for Cancer Research.

Author Manuscript Published OnlineFirst on May 12, 2021; DOI: 10.1158/0008-5472.CAN-20-2496
Author manuscripts have been peer reviewed and accepted for publication but have not yet been edited.

using Prolong Gold Antifade (ThermoFisher Scientific, Cat. P36931) and imaged (Zeiss 900 confocal microscope).

Correlation of SLC7A11 expression in human PDAC specimens with overall survival.

Immunohistochemistry analysis: Formalin-fixed, paraffin-embedded human PDAC tissue microarrays (TMAs) were obtained through the APGI (International Cancer Genome Consortium Cohort; patient demographics in **supplementary table 2**). All patients provided written informed consent. TMA rehydration and blocking for immunohistochemistry was performed as described (27-29). TMAs were probed with primary and secondary antibodies as in **supplementary table 1** followed by Vectastain® ABC kit (Vector laboratories), DAB and hematoxylin. Staining intensity in tumour and stromal compartments was scored using independent four-point scales (0-3) by two independent scorers, based on intensity in ≥75% of each compartment (normal acinar/ductal cells excluded). A consensus score was obtained for each core. For each set of 3 cores per patient, the highest tumour and stroma scores were used. Scores of 0-1 = $SLC7A11^{low}$; Scores of 2-3 = $SLC7A11^{high}$. Scores were then correlated with overall survival using a Kaplan Meier Survival Curve (see statistical analyses). Patients deceased due to other causes/still alive were censored. Non-PDAC tumours and 2 patients that lacked tumour in all 3 cores were excluded. ***RNA analysis:*** Normalised SLC7A11 expression values (expression array) were from the PACA-AU cohort through the ICGC data portal (available at: *https://dcc.icgc.org/projects/PACA-AU*). Non-PDAC patients were excluded (total PDAC patients = 242). Values were broken into tertiles (low ≤1.98, medium = 1.98-2.52, high ≥2.53) and correlated with overall survival using a Kaplan Meier Survival Curve (see statistical analyses). For comparison of SLC7A11 expression in mouse iCAFs, myCAFs and quiescent pancreatic fibroblasts we used normalised expression data from Ohlund et al (37).

siRNA transfection.

CAFs and PDAC cells were transfected with 100nM smartpool On-target plus human SLC7A11 siRNA pool (Dharmacon, Cat. L-007612-01), human SLC7A11 single sequence siRNA [Dharmacon, Cat. LU-007612-01 (part of J-007612-01)], mouse SLC7A11-siRNA (Dharmacon, Cat. L-047420-01) or non-silencing siRNA (ns-siRNA; Dharmacon, Cat. D-001810-01-50)] as described (27-29).

Downloaded from cancerres.aacrjournals.org on July 31, 2021. © 2021 American Association for Cancer Research.

Author Manuscript Published OnlineFirst on May 12, 2021; DOI: 10.1158/0008-5472.CAN-20-2496
Author manuscripts have been peer reviewed and accepted for publication but have not yet been edited.

Preparation of drugs.

Sulfasalazine (SSZ, Sigma Aldrich, Cat. S0883-10G) was dissolved in 0.1M NaOH, phosphate buffered saline (PBS), pH7.5 and filtered (0.22µm). Erastin (Cayman Chemical, Cat. 17754) and Ferrostatin-1 (Sigma-Aldrich, Cat. SML0583) were dissolved in DMSO. N-acetyl-L-cysteine (NAC; Sigma-Aldrich, Cat. A9165) was dissolved in MilliQ H_2O and filtered (0.22µm).

Cell viability assays.

Cell proliferation or viability was measured by trypan blue exclusion and cell counting kit 8 (CCK8) assays as described (27-29) at: (i) 72h post-transfection with siRNA; (ii) 48h post-treatment with 0.2-0.4mM SSZ; (iii) 24-48h post-treatment with 40µM erastin; (iv) 72h post-seeding of shRNA stable lines. *Co-treatments:* (i) 0-60µM tert-butyl hydroperoxide (tBHP; oxidative stress inducer; Sigma Aldrich, Cat. 458139) in the final 24h of assays; (ii) 0-66µM 2-mercaptoethanol (2-ME) in parallel with SSZ; (iii) 2µM Ferrostatin in the final 24h of assays; (iv) Low nutrient conditions for the final 24h of assays: Serum-free Plasmax™, no serum, 2mM glutamine (refer to https://ximbio.com/reagent/156371/plasmaxsuptmsup-cell-culture-medium for comparison of Plasmax™ and IMDM).

Cell cycle, cell death and senescence assays.

Ferroptosis assay: Adhered CAFs (i) 72h post-transfection with siRNA, (ii) 48h post-seeding of stable shRNA CAFs, (iii) 9h post-treatment with 40 µM erastin or 0.2% DMSO (control) were assayed for ferroptosis using Glutathione Peroxidase Assay Kit (Abcam, Cat. ab102530). **Cell cycle assay (72h post-transfection):** Cell cycle analysis was performed by propidium iodide (PI) staining and flow cytometry on a BD LSR Fortessa™, as described (29). **Cell senescence assay (72h post-transfection or SSZ treatment):** Senescence was assessed using a Senescence β-galactosidase Cell Staining Kit (Cell Signaling Technologies, Cat. 9860). **Measurement of autophagy (72h post-transfection):** Western blot was performed for Light Chain 3 isoform B (LC3B), to check for conversion from cytosolic LC3BI to autophagosome-bound LC3BII. Western blot was performed as per SLC7A11 procedure, except samples were boiled. Western blots were probed with antibodies described in **supplementary table 1** then visualised and quantified as per SLC7A11 Western blot. **Apoptosis assay (72h post-transfection, 24h post-**

Downloaded from cancerres.aacrjournals.org on July 31, 2021. © 2021 American Association for Cancer Research.

Author Manuscript Published OnlineFirst on May 12, 2021; DOI: 10.1158/0008-5472.CAN-20-2496
Author manuscripts have been peer reviewed and accepted for publication but have not yet been edited.

tBHP): Adherent and floating cells were collected and total apoptosis detected using an AnnexinV-PE/7AAD kit (BD Bioscience, Cat. 559763) according to manufacturer's instructions and analysed on a BD LSR Fortessa™.

Measurement of cystine uptake.

Non-transfected CAFs (SSZ experiments) or CAFs, 48h post-transfection with siRNA, were seeded at 15,000 cells/well into Wallac isoplate 96–well plates. The following day, cystine uptake was assayed immediately (knockdown experiments) or 2-3h post-treatment with SSZ (SSZ maintained during assay). Cystine uptake was measured as described (38).

Assessing glutathione synthesis, oxidative stress and glutamate efflux.

Measurement of intracellular glutathione: Intracellular glutathione was measured in whole cell lysates [prepared: (i) 72h post-transfection with siRNA; (ii) 72h post-seeding of shRNA stable lines; (iii) after 48h 0.25mM SSZ; (iv) 16h post-0.25mM SSZ with or without 1mM NAC] using ApoGSH™ Glutathione Colorimetric Assay (BioVision, Cat. K261-100) or Glutathione Assay Kit (Cayman Chemical, 703002) according to manufacturer's instructions. **Detection of intracellular ROS using CellROX:** 72h post-transfection or after addition of 0.4mM SSZ, CAFs were incubated with 325μM tBHP for 1h. CAFs were then stained with CellROX green reagent (Life Technologies, C10444) according to manufacturer's instructions. Fluorescence was analysed on a BD LSRFortessa™. **Glutamate efflux assay:** 72h post-transfection, CAFs were washed and cultured in M2 buffer (Sigma Aldrich) for 4h. Glutamate was measured in cell supernatant using Amplex Red Glutamic Acid/Glutamate Oxidase Assay Kit (Thermofisher Scientific; Cat. A12221) . Fluorescence measured using an EnSpire Multimode Plate Reader (PerkinElmer) at 571/586nm (excitation/emission).

Metabolomics for intracellular cystine and glutamate

To assess glutamate:cystine exchange, immortalised CAFs expressing shRNA were cultured in glutamine-free IMDM (Sigma), 10% dialysed FBS, 4mM $^{13}C_5$-glutamine (Sigma) for 24h. Cells

Downloaded from cancerres.aacrjournals.org on July 31, 2021. © 2021 American Association for Cancer Research.

Author Manuscript Published OnlineFirst on May 12, 2021; DOI: 10.1158/0008-5472.CAN-20-2496
Author manuscripts have been peer reviewed and accepted for publication but have not yet been edited.

were washed twice and medium replaced with complete culture medium, 10% dialysed FBS. Cell extracts were harvested by scraping into cold lysis medium (methanol: acetonitrile: MilliQ water at 50:30:20 v/v) and debris pelleted at ≥14,000g, 15min, 4^{o}C. The supernatant was then used for LC-MS analysis as described (39). Metabolites were predetermined with in-house standards (20-40µM, HPLC-grade, Sigma). Labelling patterns were analysed by Xcalibur (v4.1, Thermo Fisher Scientific; RRID:SCR_014593) and mass of isotopomers corrected against naturally occurring stable carbons.

3D co-culture models.

Spheroid outgrowth assay: MiaPaCa-2 PDAC cells and patient-derived CAFs were transfected with siRNA. After 24h, 2500 of each was co-seeded in suspension, spheroids formed over 24h under normal culture conditions, then transferred to 0.33% soft-agarose medium (20% FBS, 4% L-glutamine, 0.33% agarose in low glucose DMEM:F12 medium) and overlayed on 50µL pre-set 0.5% soft-agarose medium in a 96-well round-bottom plate. **Spheroid growth assay:** PDAC cells and immortalised CAFs expressing shRNA were seeded into low adherence round-bottom 96-well plates (2500 PDAC cells + 7500 CAFs). After 24h culture to allow spheroid formation, supernatant on spheroids was replaced with 1:1 complete culture medium:Corning® Matrigel® (In Vitro Technologies, Cat. 354230) then returned to culture. Daily brightfield photos were taken on an inverted light microscope and spheroid growth/outgrowth quantified using ImageJ (RRID:SCR_003070).

Matrix contractility assay.

Organotypic assays were adapted from published protocols (40). 0.3-1x10^{5} CAFs (n=4, 24h post-transfection) were embedded in 1.25 mL of rat-tail collagen I. Once polymerised, fibroblast-collagen matrices were allowed to contract in IMDM, 10% FBS, 4 mM L-glutamine, 1% penicillin/streptomycin for six days with images taken at Days 2-6. Collagen plug area was quantified from brightfield images. At Day 6, collagen matrices were fixed, paraffin embedded and sectioned for Second Harmonic Generation (SHG) analysis as described (40,41). SHG signal was acquired (line average:16) and intensity/grey-level co-occurrence matrix (GLCM) analysis performed in Matlab (Mathworks; RRID:SCR_001622) as described (40,41). Paraffin-embedded samples were cut into 4µm sections and stained with 0.1% picrosirius red (Polysciences)

Downloaded from cancerres.aacrjournals.org on July 31, 2021. © 2021 American Association for Cancer Research.

Author Manuscript Published OnlineFirst on May 12, 2021; DOI: 10.1158/0008-5472.CAN-20-2496
Author manuscripts have been peer reviewed and accepted for publication but have not yet been edited.

according to manufacturer's instructions. Polarised light imaging and intensity measurement was performed as described (40,41).

Transgenic pancreatic cancer mouse models and genetic ablation of SLC7A11.

Transgenic mouse studies were approved by the local ethical review committee at University of Glasgow according to UK Home Office regulations (licence: 70/8646). KC (Kras-mutated) and KPC (Kras- and p53-mutated) mouse models (42) [Alleles used: Pdx-1-promoter, lox-stop-lox-KrasG12D/+ allele, and lox-stop-lox-Trp53R172H/+ ± *Slc7a11*$^{fl/fl}$ (IMPC (MGI:1347355)] were genotyped by Transnetyx (Cordoba, TN, USA). In these models, expression of mutated Kras, P53, and conditional deletion of SLC7A11 are driven by Pdx1-Cre, meaning that SLC7A11 is lost only from the epithelial cells of the pancreas. *Pancreatic intraepithelial neoplasia (PanIN) scoring*: *Slc7a11*$^{+/+}$ (KC) and *Slc7a11*$^{fl/fl}$ (KC with conditional *Slc7a11* knockout) mice were sampled at 70 days old and PanINs scored from whole H&E sections (normalised to mm^2). *Survival:* KPC and KPC *Slc7a11*$^{fl/fl}$ mice were monitored thrice weekly and sampled when exhibiting clinical signs of PDAC (abdominal swelling, jaundice, hunching, piloerection and weight loss). RNA *in situ* hybridisation (ISH) was performed on formalin-fixed KPC tumour sections. RNA ISH (RNAscope) was performed according to the manufacturer's protocol (ACD RNAscope 2.0 High Definition–Brown) for *Slc7a11* (Basecope probe targets floxed exon 3). Western blot was performed as above, using antibodies in **supplementary table 1**.

Star nanoparticle synthesis.

Star nanoparticles (Star 3) were synthesised as described (43).

Sub-cutaneous and orthotopic pancreatic cancer mouse models.

All mouse studies were approved by the UNSW Sydney animal care and ethics committee (approval: ACEC 16/25B, ACEC 19/3A). **Sub-cutaneous model:** TKCC5 PDAC cells were co-implanted with immortalised CAFs expressing shRNA (10^6 each) into the flank of 8 week-old female BalbC nude mice in 1:1 mix of PBS and matrigel. Tumour growth was monitored by calliper measurement. **Orthotopic model (stable shRNA cell lines):** Luciferase-expressing MiaPaCa-2 cells (27) and immortalised CAFs expressing shRNA (as per spheroids) were co-implanted (10^6 each) into the pancreas tail of 8 week-old female BalbC nude mice, as described

Downloaded from cancerres.aacrjournals.org on July 31, 2021. © 2021 American Association for Cancer Research.

Author Manuscript Published OnlineFirst on May 12, 2021; DOI: 10.1158/0008-5472.CAN-20-2496
Author manuscripts have been peer reviewed and accepted for publication but have not yet been edited.

(27,34). Tumour volume was measured weekly by ultrasound on a VisualSonics Vevo 3100 from week 4 post-implant. Mice that had no measurable tumour at week 4 were excluded (1 exclusion). **Orthotopic model (therapeutic knockdown):** As above except cells did not express shRNA. ***Star 3-siRNA gene silencing efficiency study:*** 6-weeks post-surgery, mice were treated with 3mg/kg control-siRNA (antisense: 5'-GAACUUCAGGGUCAGCUUGCCG) or SLC7A11-siRNA (antisense: 5'-AGACCCAAUAAGUUUGCCG) complexed to Star 3, intravenously once daily for three days. ***Star 3-siRNA therapeutic study:*** 4 weeks post-surgery, mice were randomised based on luminescence as described (27), then treated with 3mg/kg Star 3+siRNA, intravenously daily for the first three days, followed by twice weekly for 4 weeks. Mice were co-treated intravenously with 10mg/kg Abraxane® (Specialised Therapeutics Australia) or 90mg/kg human albumin (control), once weekly for 4 weeks. At end points, mice were humanely euthanised and organs/tumours harvested. Tumour volume was calculated by calliper measurement with operator blinded to treatment. Tumour fragments were 4% paraformaldehyde-fixed and paraffin embedded, or frozen in Tissue-Tek® Optimal Cutting Temperature Compound (OCT, VWR International). Metastases were detected by *ex vivo* luminescence (>600 counts) and confirmed by H&E as described (27).

Measurement of collagen content and organisation in pancreatic tumour sections (orthotopic and transgenic PDAC models).

Picrosirius red staining and measurement of total collagen content and fibril density (polarised light analysis): 5μm sections of paraffin-embedded tumours were stained with 0.1% picrosirius red and counter-stained with methyl green or hematoxylin. Collagen content was calculated from representative regions (percent of area picrosirius red positive/region excluding necrosis, average tumour coverage = 13%) using ImageJ (RRID:SCR_003070) or Qupath, then averaged for each tumour. Polarised light analysis was performed on the same regions, aas described (40,41). ***Second harmonics analysis of collagen organisation and directionality*:** SHG signal was acquired in OCT-embedded tumour sections (15 μm) and maximum intensity projections used for GLCM and orientation analyses (3 representative regions [775μmx775μm]/tumour) as described (40,44,45).

Downloaded from cancerres.aacrjournals.org on July 31, 2021. © 2021 American Association for Cancer Research.

Author Manuscript Published OnlineFirst on May 12, 2021; DOI: 10.1158/0008-5472.CAN-20-2496
Author manuscripts have been peer reviewed and accepted for publication but have not yet been edited.

Immunohistochemistry for SLC7A11, Alpha Smooth Muscle Actin (αSMA) and CD31 in mouse PDAC tumours.

Immunohistochemistry was performed in paraformaldehyde-fixed and paraffin-embedded tumour sections, as described (27-29) using antibodies in **supplementary table** 1. SLC7A11 staining intensity, αSMA area coverage and CD31-positive blood vessels (open vs closed manual count) were analysed in representative images (excluding necrosis) using colour deconvolution in ImageJ (RRID:SCR_003070), then averaged per tumour. SLC7A11 staining intensity was calculated from 3 images/tumour (average tumour coverage = 10%). Optical density (staining intensity) = log[maximum intensity of pixels/average intensity of pixels]. αSMA representative regions average tumour coverage was 21%. CD31-positive representative regions average tumour coverage was 55%. Observers were blinded to treatments.

3D human PDAC tumour explant model.

Human PDAC tumour specimens were obtained from patients undergoing pancreaticoduodenectomy at Prince of Wales Hospital or Prince of Wales Private Hospital, Randwick, NSW, Australia. All patients provided written informed consent through the Health Science Alliance Biobank, all work was approved by UNSW human ethics (HC180973), and all experiments were performed in accordance with the relevant regulations. Patient-derived explants (1-8 mm^3) were established and cultured for 12 days with daily medium change, as described (46). Star 3 nanoparticles (60 μg) complexed to siRNA were added to the reservoir as described (46) on days 0, 3, 6, 9. Alternatively, 400 μM sulfasalazine or vehicle was added to the reservoir on days 0, 3, 6, 9. Patient-derived explants were treated with 10 μM BrdU substrate (BD Biosciences, Cat. 550891) for 24h prior to fixation (day 12), as described (46).

Statistical Analyses.

Statistical comparisons were performed using two-tailed student t-test (2 groups) or ANOVA (≥3 groups; post-hoc tests: Dunn's, Sidak's multiple comparison) using GraphPad Prism (RRID:SCR_002798). Comparisons of univariate time to event (survival) were performed using the log-rank test and hazard ratios calculated from the Cox proportional hazards (PH) model. Multivariate associations between variables and time to event were contained from PH regression and survival curves calculated using the method of Kaplan-Meier (KM). Where

Downloaded from cancerres.aacrjournals.org on July 31, 2021. © 2021 American Association for Cancer Research.

Author Manuscript Published OnlineFirst on May 12, 2021; DOI: 10.1158/0008-5472.CAN-20-2496
Author manuscripts have been peer reviewed and accepted for publication but have not yet been edited.

tumour and stroma scores correlated with outcome, baseline variables associated with predicting scores were examined by multivariate logistic regression. Tumour grade was excluded from multivariate analyses as it did not correlate with overall survival in our cohort due to the low percentage of grade 3-4 tumours (13% of cohort). Survival analyses were performed using Analysis of Censored and Correlated Data (ACCoRD; RRID:SCR_009015) V6.4 Boffin. A p-value ≤ 0.05 was considered statistically significant.

RESULTS

High stromal SLC7A11 expression in human PDAC specimens predicted poor overall survival.

Results showed that SLC7A11 and its partner SLC3A2 mRNA levels are upregulated in PDAC patient-derived CAFs compared to patient-derived non-cancerous pancreatic fibroblasts (**Figure 1A**). Similar results were obtained when we analysed Ohlund et al data (37), which showed SLC7A11 mRNA expression was increased in iCAF (2.7-fold) and myCAF (1.6-fold) sub-populations versus quiescent pancreatic stellate cells (**Supplementary Table 3**). We confirmed that all human PDAC CAFs expressed SLC7A11 protein (**Figure 1B**). SLC7A11 protein levels in human CAFs (5/6 CAFs tested) were comparable to PDAC cells with the highest SLC7A11 expression (HPAFII, ASPC1) (**Figure 1B**). SLC7A11 protein levels were higher in PDAC cells derived from metastatic sites (HPAFII/AsPC1) relative to those from primary tumour sites (MiaPaCa2/Panc-1) (**Figure 1B**). Co-immunofluorescence staining for SLC7A11 and αSMA (CAF marker) in human PDAC tumours demonstrated abundant SLC7A11 protein in αSMA positive CAFs (**Figure 1C**). We next scored SLC7A11 protein expression, as determined by immunohistochemistry, in tumour and stromal compartments of human PDAC tissue microarrays (**Figure 1D**; independent scoring scales used for tumour and stroma) and correlated with overall patient survival (**Figure 1E-G**). 58% of patients were Tumour^{high} (**Figure 1E**) and 47% were Stroma^{high} (**Figure 1F**). SLC7A11 expression in the PDAC tumour compartment alone did not predict patient survival (**Figure 1E**). Similar results were obtained when we analysed the ICGC publicly available mRNA data (47) (**Figure S1G**). Importantly, in a multivariate logistic regression, high SLC7A11 in the stroma was independently prognostic of

Downloaded from cancerres.aacrjournals.org on July 31, 2021. © 2021 American Association for Cancer Research.

Author Manuscript Published OnlineFirst on May 12, 2021; DOI: 10.1158/0008-5472.CAN-20-2496
Author manuscripts have been peer reviewed and accepted for publication but have not yet been edited.

poorer overall survival (**Figure 1F**, p=0.041, Hazard ratio=1.45; **Supplementary Table 4**), when adjusted for vascular invasion. In addition, we identified a sub-group of patients (Tumour^{low}Stroma^{high}) that had significantly poorer overall survival compared to all other score combinations (**Figure 1G-H**).

Inhibition of SLC7A11 in CAFs reduced cell proliferation and metabolically rewired CAFs.

To assess SLC7A11 function in CAFs, we used siRNA and two pharmacological inhibitors [Sulfasalazine (SSZ), Erastin]. SLC7A11-siRNA reduced mRNA (**Figure S1H**) and protein levels (**Figure S1C-D**) compared to control-siRNA. Inhibition of SLC7A11 by siRNA, SSZ or erastin significantly decreased CAF proliferation and viability (**Figure 2A-C**) including under low nutrient conditions (30.6±13.8% reduction in live cells relative to ns-siRNA; $p \leq 0.05$, n=3). Importantly, SLC7A11 knockdown in CAFs inhibited proliferation in both SLC7A11^{low} and SLC7A11^{high} CAFs (**Figure S2A**), indicating SLC7A11 is functionally essential in CAFs regardless of expression level. 2-mercaptoethanol (2-ME), which facilitates bypass of xCT for cysteine (45), rescued CAF growth in the presence of SSZ (**Figure 2B)**. This indicated that SSZ-induced growth arrest of CAFs was due to cystine starvation. Indeed, treatment of CAFs with SLC7A11-siRNA or SSZ significantly reduced cystine uptake (**Figure 2D-E**) and intracellular glutathione (**Figure 2F-G**), relative to controls. The reduction in glutathione was rescued by addition of N-acetyl-cysteine (NAC; **Figure 2G**), which provides an SLC7A11-independent source of cysteine. Stable knockdown of SLC7A11 (**Figure S1E-F**) in hTERT-immortalised CAFs using shRNA similarly decreased intracellular cystine and increased glutamate retention, consistent with SLC7A11 inhibition (**Figure S2B-C**).

We validated previous findings that both SSZ and erastin significantly decreased MiaPaCa-2 PDAC cell proliferation (**Figure S2D-E**) and SSZ inhibition can be rescued by 2-ME (18). In contrast to results in PDAC cells and CAFs, SLC7A11 knockdown (**Figure S2F**) had minimal effect on the viability of non-tumour human pancreatic ductal epithelial cells (**Figure S2G**).

We next assessed intracellular reactive oxygen species (ROS; oxidative stress) and found that SLC7A11 knockdown using siRNA in CAFs had no effect on intracellular ROS in the absence of stress, but significantly increased intracellular ROS in the presence of stress (tBHP) (**Figure 2H;** tBHP increased mitochondrial ROS, **Figure S3A**), suggesting decreased anti-oxidant

Downloaded from cancerres.aacrjournals.org on July 31, 2021. © 2021 American Association for Cancer Research.

Author Manuscript Published OnlineFirst on May 12, 2021; DOI: 10.1158/0008-5472.CAN-20-2496
Author manuscripts have been peer reviewed and accepted for publication but have not yet been edited.

capacity. In contrast, SSZ treatment alone increased intracellular ROS in CAFs, to levels where tBHP treatment had no significant additive effect on intracellular oxidative stress (**Figure 2I**). Note that the lack of an increase in intracellular ROS with tBHP alone is due to the short incubation time (1 hour) for this assay. SLC7A11 knockdown in CAFs had no effect on glutamate secretion (**Figure S3B**).

Inhibition of SLC7A11 increased sensitivity to oxidant stress and ferroptosis.

We confirmed SLC7A11 knockdown was maintained in the presence of oxidative stress (**Figure S3C**) and observed that oxidative stress increased SLC7A11 protein expression in cells treated with control siRNA (**Figure S3C**). Knockdown of SLC7A11 using siRNAs in CAFs sensitised them to external oxidant stress (tert-butyl hydroperoxide, tBHP) by decreasing viability (**Figure 2J**) and increasing apoptosis (**Figure 2K, Figure S3D**). Previous studies have shown that SLC7A11 inhibition in PDAC cells induces oxidative stress-induced cell death (ferroptosis; (21,23,48)). We observed that inhibition of SLC7A11 with erastin reduced glutathione peroxidase activity indicative of ferroptosis in CAFs (**Figure 2L**). Importantly, the ferroptosis inhibitor ferrostatin rescued CAFs from the anti-proliferative effects of erastin confirming ferroptosis (**Figure 2M**). Likewise, stable SLC7A11 knockdown in CAFs decreased cell viability in the presence of oxidant stress (**Figure 2N**) and increased ferroptosis (i.e. decreased glutathione peroxidase activity, **Figure 2O**).

SLC7A11 inhibition increased senescence of CAFs in the absence of stress.

Given SLC7A11-siRNA alone had no effect on apoptosis, we explored other anti-proliferative mechanisms. We showed that SLC7A11-siRNA had no effect on autophagy (**Figure S3E**), but increased CAFs in S-phase of cell cycle (**Figure S3F**, suggesting hindered S phase progression). SLC7A11 knockdown or SSZ treatment in CAFs also significantly increased senescence (**Figure 2P-Q**). Results showed that SLC7A11 knockdown in CAFs induced senescence and in the presence of additional oxidative stress compromised CAF survival.

SLC7A11 inhibition decreased CAF and PDAC co-culture spheroid growth *in vitro*.

To determine whether SLC7A11 inhibition in CAFs affected their ability to support PDAC cell growth we performed 3D co-culture assays [spheroid outgrowth (**Figure 3A**) and spheroid

Downloaded from cancerres.aacrjournals.org on July 31, 2021. © 2021 American Association for Cancer Research.

Author Manuscript Published OnlineFirst on May 12, 2021; DOI: 10.1158/0008-5472.CAN-20-2496
Author manuscripts have been peer reviewed and accepted for publication but have not yet been edited.

growth assays (**Figure 3B**)]. Transient knockdown of SLC7A11 in either CAFs, PDAC cells, or both significantly reduced spheroid outgrowth (**Figure 3C**). Importantly, knockdown of SLC7A11 in CAFs alone or in both cell types was more effective at inhibiting spheroid outgrowth than SLC7A11 knockdown in PDAC cells alone (**Figure 3C**). Using a stable knockdown approach in MiaPaCa2 PDAC cells and immortalised CAFs, in a 3D matrigel-embedded spheroid assay, we observed similar results (**Figure 3D**). Except SLC7A11-shRNA in MiaPaCa-2 PDAC cells alone had no effect on spheroid growth. In contrast, SLC7A11-shRNA in CAFs alone or in both PDAC cells and CAFs reduced spheroid size (relative to start) at endpoint by 40% (**Figure 3D**). We repeated the assay using the CAF shRNA lines above combined with additional PDAC cells (Panc-1, AsPC1, TKCC5) and observed a comparable reduction in spheroid growth relative to CAF(control-shRNA) spheroids (**Figure 3E-G**).

SLC7A11 inhibition decreased collagen remodelling *in vitro*.

SLC7A11 knockdown in CAFs significantly reduced contraction of collagen plugs over 6 days (**Figure 3H;** higher contraction = greater remodelling). Brightfield analysis of picrosirius red-stained collagen plugs demonstrated that collagen plugs remodelled by CAFs transfected with SLC7A11-siRNA had decreased collagen relative to controls (**Figure 3I**). Polarised light analysis (measures density of collagen fibrils) showed that plugs remodelled by CAFs transfected with SLC7A11-siRNA decreased overall birefringent fibrils (**Figure 3J**) and high/medium density fibrils, and increased low density fibrils, relative to controls (**Figure 3K**). This was confirmed by Second Harmonics Generation (SHG) analysis of fibrillar collagen (**Figure 3L**). Fibril organisation was also assessed by Grey-Level Co-Occurrence Matrix (GLCM) analysis of SHG images but showed no significant difference between ns-siRNA and SLC7A11-siRNA groups (**Figure 3L**).

Genetic ablation of SLC7A11 in PDAC cells only had no effect on tumour growth in genetically engineered mouse models.

Results above suggested that the presence of CAFs would likely influence the effect of an SLC7A11 inhibition approach *in vivo*. We assessed the impact of genetic ablation of SLC7A11 driven by an epithelial-specific promoter (*Slc7a11*$^{fl/fl}$, does not affect CAFs), in two transgenic mouse models of PDAC [KC and KPC (42)]. *Slc7a11* knockout was confirmed by RNA *in situ*

Downloaded from cancerres.aacrjournals.org on July 31, 2021. © 2021 American Association for Cancer Research.

Author Manuscript Published OnlineFirst on May 12, 2021; DOI: 10.1158/0008-5472.CAN-20-2496
Author manuscripts have been peer reviewed and accepted for publication but have not yet been edited.

hybridisation and Western blot (**Figure 4A-B**). We observed no significant difference in PanIN formation between control and *Slc7a11*$^{fl/fl}$ KC mice (**Figure 4C**). Similarly, in KPC mice we observed no difference in survival (**Figure 4D**) or intratumoural αSMA-positive CAFs (**Figure 4E**), but did note a significant decrease in intratumoural collagen in KPC *Slc7a11*$^{fl/fl}$ mice, relative to controls (**Figure 4F**). *In vitro*, we observed higher basal expression of SLC7A11 was observed in KPC PDAC cells relative to CAFs (**Figure S4A**). Consistent with *in vivo* results, transient SLC7A11 knockdown *in vitro* (**Figure S4B-C**) had no effect on KPC PDAC cell proliferation (**Figure 4G**) but significantly reduced proliferation of KPC CAFs (**Figure 4H**).

Stable knockdown of SLC7A11 in both human PDAC cells and CAFs is required to reduce tumour growth, metastatic spread and fibrosis.

We performed a sub-cutaneous model to assess the effect of SLC7A11 knockdown in hTERT immortalised CAFs in combination with a patient-derived PDAC cell line (TKCC5). Stable SLC7A11 knockdown in CAFs substantially reduced tumour incidence (**Figure 5A**). To further delineate the contribution of PDAC cells and CAFs to the anti-tumour effects of SLC7A11 knockdown, we orthotopically implanted MiaPaCa-2 PDAC cells and immortalised CAFs expressing control-shRNA or SLC7A11-shRNA into the pancreas of host mice. SLC7A11 knockdown in either PDAC cells alone, CAFs alone or both reduced PDAC tumour growth (**Figure 5B**). SLC7A11 knockdown in PDAC cells alone or in both cell types significantly reduced metastasis (**Figure 5C**). SLC7A11 knockdown in CAFs alone or in both cell types significantly reduced intratumoural collagen (fibrosis; **Figure 5D**). In addition, SLC7A11 knockdown in either PDAC cells or CAFs alone trended towards decreased fibrosis (**Figure 5D**) and metastases (**Figure 5C**), respectively, though this was not significant.

Gene silencing nanoparticles targeting SLC7A11 decreased orthotopic tumour growth, CAF activity and fibrosis.

To overcome the physical barrier of fibrosis and deliver SLC7A11-siRNA to PDAC mouse tumours we used Star 3 nanoparticles (43). Star 3+SLC7A11-siRNA decreased SLC7A11 protein levels in orthotopic pancreatic tumours (**Figure 6A**). The therapeutic efficacy of Star 3+SLC7A11-siRNA was then assessed using a therapeutic regimen on tumours randomised based on luminescence (**Figure S4D**), with or without Abraxane® (human albumin-bound

Downloaded from cancerres.aacrjournals.org on July 31, 2021. © 2021 American Association for Cancer Research.

Author Manuscript Published OnlineFirst on May 12, 2021; DOI: 10.1158/0008-5472.CAN-20-2496
Author manuscripts have been peer reviewed and accepted for publication but have not yet been edited.

paclitaxel; **Figure 6B**). Whilst Abraxane® treatment did not affect tumour growth, SLC7A11 inhibition alone, or in combination, significantly decreased tumour growth (**Figure 6C**). In addition, SLC7A11 knockdown alone led to the greatest reduction in the incidence of mice with metastasis (50% in control-siRNA+albumin; 37.5% in control-siRNA/SLC7A1-siRNA+Abraxane; 28.6% in SLC7A11-siRNA+albumin), but had no effect on the number of metastases per mouse (**Figure 6D**). Furthermore, Star 3+SLC7A11-siRNA significantly decreased intratumoural αSMA positive cells (**Figure 6E**) and picrosirius red staining (fibrosis), relative to controls (**Figure 6F**), though fibril density and organisation were not significantly affected (**Figure S4E-G**). This resulted in an increase in the fraction of open CD31-positive blood vessels, relative to controls (**Figure 6G**), suggesting normalisation of intratumoural vasculature.

SLC7A11 inhibition in 3D human PDAC tumour explants decreased activated CAFs and proliferation.

We silenced (Star 3+SLC7A11-siRNA) or inhibited (sulfasalazine) SLC7A11 in 3D human PDAC tumour explants obtained from surgical resections (**Figure 7A**). This model retains 3D organisation and interactions of PDAC cells and stromal cells for up to 12 days in a tissue culture dish (46). Knockdown of SLC7A11 significantly decreased activated CAFs, cytokeratin-positive tumour cells, and cell proliferation relative to controls (**Figure 7B-E**). Using an orthogonal approach (SSZ) we observed a similar reduction in activated CAFs and cell proliferation relative to controls (**Figure 7F-G**).

DISCUSSION

In this study, we showed for the first time that high SLC7A11 expression in the stroma of human PDAC tumours predicts poorer patient survival. A key finding of this study is the importance of SLC7A11 in regulating the growth and function of CAFs, and that inhibiting SLC7A11 in CAFs is essential to maximise the full therapeutic benefit of targeting SLC7A11 in PDAC.

High SLC7A11 expression has been reported to predict poorer survival in different tumour types (15,49,50). However, the role of SLC7A11 in PDAC is less clear. Maurer et al (51) and more

Downloaded from cancerres.aacrjournals.org on July 31, 2021. © 2021 American Association for Cancer Research.

Author Manuscript Published OnlineFirst on May 12, 2021; DOI: 10.1158/0008-5472.CAN-20-2496
Author manuscripts have been peer reviewed and accepted for publication but have not yet been edited.

recently Badgley et al (23) observed significantly higher levels of SLC7A11 mRNA in the PDAC epithelial compartment relative to stroma. We found that SLC7A11 mRNA expression did not correlate with overall survival, but that high SLC7A11 protein in the stroma (but not tumour), was prognostic of poorer patient survival (APGI ICGC cohort). Our results highlight that segregation of tumour and stroma is a critical consideration in any prognostic analysis for PDAC. Interestingly, we identified a sub-population of patients ($Tumour^{SLC7A11low}Stroma^{SLC7A11high}$) that had the poorest overall survival which may suggest unique PDAC cell:CAF metabolic dependencies that drive more aggressive disease and requires further investigation. Our results highlight that despite the higher average expression of SLC7A11 in the tumour compartment, expression in the PDAC stroma may be functionally significant for disease progression. In addition, a retrospective analysis of gene expression array data from (37) showed that SLC7A11 expression was elevated in myCAFs and iCAFs, opening an avenue for future investigations into the immune modulatory role of SLC7A11 in iCAFs.

Functional inhibition (knockdown vs drug) of SLC7A11 in CAFs reduced their proliferation and induced cell death including ferroptosis. Interestingly both SLC7A11 knockdown and SSZ treatment in CAFs induced senescence, which may have been a response to amino acid deprivation and hindered protein synthesis. Indeed, Daher et al (21) demonstrated that SLC7A11 knockout in PDAC cells induced an amino acid stress response. We confirmed that SLC7A11 inhibition significantly hindered cystine uptake and GSH. A key point of difference between siRNA-based and SSZ-based approaches was that SLC7A11 knockdown alone did not significantly increase oxidative stress in CAFs, whereas SSZ did. A potential explanation is that SSZ can decrease levels of additional enzymes and signalling involved in oxidative stress protection (52-54), which might induce oxidative stress more rapidly than knockdown. Our results highlighted the crucial dependence of CAFs on SLC7A11 for cystine uptake and GSH synthesis.

Stable SLC7A11 knockdown in immortalised CAFs combined with multiple PDAC lines reduced spheroid growth, implying that SLC7A11 targeting in CAFs may be beneficial regardless of tumour cell heterogeneity. The lack of effect observed with SLC7A11 knockdown in PDAC cells alone may have been due to their reliance on CAFs for spheroid formation and the 3-fold excess of CAFs, potentially placing more emphasis on the role of CAFs. This is implied

Downloaded from cancerres.aacrjournals.org on July 31, 2021. © 2021 American Association for Cancer Research.

Author Manuscript Published OnlineFirst on May 12, 2021; DOI: 10.1158/0008-5472.CAN-20-2496
Author manuscripts have been peer reviewed and accepted for publication but have not yet been edited.

by our spheroid outgrowth assay, whereby SLC7A11 knockdown in PDAC cells was equally effective to knockdown in CAFs with equal cell ratios. Given our immortalised CAFs had adapted to stable SLC7A11 knockdown (no anti-proliferative effect), it is likely our observations are a consequence of reducing paracrine pro-tumour signals from CAFs in addition to potentially reducing CAF survival under more stressful conditions than a 2D mono-culture. Furthermore, SLC7A11 knockdown reduced CAF-mediated remodelling of 3D collagen *in vitro,* suggesting this approach might help overcome a PDAC drug delivery barrier.

The anti-fibrotic effect of conditional SLC7A11 knockout in KPC tumours, in the absence of a survival benefit, implied pro-fibrogenic cross-talk between tumour and stromal cells had been disrupted. This was also reflected in *in vitro* proliferation assays. Our results are in contrast to prior KPC studies in which SLC7A11 inhibition or genetic ablation (22,23) significantly reduced tumour growth. A key difference is that these prior studies did not selectively target PDAC cells making it possible that CAFs were affected. We can directly compare our results to those of Badgley et al (23) who utilised KPC mice with deletion of SLC7A11 under temporal control of tamoxifen and driven from the Rosa26 locus, meaning that SLC7A11 is lost from tumour and stroma. In contrast, our model specifically ablated SLC7A11 in pancreatic epithelial cells. These differences support our hypothesis regarding the importance of SLC7A11 in the PDAC microenvironment. However, the difference may also be explained by selection of PDAC cells resistant to SLC7A11inhibition from tumour initiation.

In an orthotopic PDAC mouse model, stable SLC7A11 knockdown in PDAC cells, immortalised CAFs or both reduced PDAC tumour growth, implying that CAFs and PDAC cells are equally important targets for SLC7A11 inhibition. Importantly, SLC7A11 knockdown in PDAC cells alone significantly reduced metastasis while knockdown in CAFs significantly decreased fibrosis, with the dual knockdown group exhibiting both. We also observed trends (although not significant) towards decreased fibrosis and metastases in the PDAC only and CAF only groups, respectively. The results again highlight that dual inhibition of PDAC cells and CAFs is important to maximise stromal remodelling and anti-metastatic effects, but that inhibition of SLC7A11 in either compartment has the potential to interfere with pro-tumour cross-talk. While the outcome is consistent with anti-tumour effects observed in prior studies (22,23), our results appear to be at odds with our KPC model findings and *in vitro* spheroid results. These

Downloaded from cancerres.aacrjournals.org on July 31, 2021. © 2021 American Association for Cancer Research.

Author Manuscript Published OnlineFirst on May 12, 2021; DOI: 10.1158/0008-5472.CAN-20-2496
Author manuscripts have been peer reviewed and accepted for publication but have not yet been edited.

differences are likely explained by species and experimental approach. In contrast to human PDAC cells, SLC7A11 knockdown in KPC PDAC cells had no effect on proliferation, suggesting mouse KPC PDAC cells are more resistant to this approach. In our spheroid assay, as discussed above, we utilised an excess of and were dependent on CAFs for spheroid formation, potentially placing a heavier emphasis on the role of CAFs.

Our findings collectively demonstrate that SLC7A11 knockdown in PDAC cells or CAFs has the potential to reduce tumour growth and fibrosis, and that the most effective therapeutic approach is to inhibit SLC7A11 in both. Our results also indicate that SLC7A11 inhibition might interfere with pro-tumour cross-talk between PDAC cells and CAFs. While we cannot confirm as yet the central cross-talk mechanism(s) that are influenced, these may encompass: (i) reducing activated CAF numbers available to support tumour cells; (ii) directly or indirectly interfering with fibrosis production/remodelling by CAFs; (iii) inhibiting secretion of pro-survival signalling molecules; (iv) interfering with metabolic cross-talk that could help support survival of both cell types in the nutrient-poor tumour microenvironment. This will be the subject of future studies.

To complement prior work highlighting the potential of SLC7A11 inhibition as a therapeutic approach (22,23), we again used an orthotopic model, with a defined pre-mortality endpoint to allow for time-matched comparison of CAF activation, fibrosis and tumour size. We used a polymeric nanoparticle (Star 3) that we developed to package SLC7A11-siRNA and overcome physical barriers to drug delivery in PDAC (43). Our nanoparticle accumulates in PDAC tumours without specific targeting, but is rapidly cleared from normal organs, minimising the chance for off-target toxicity (43). Star 3+SLC7A11-siRNA decreased tumour growth and reduced the incidence of mice with metastases, although metastases per mouse were not significantly reduced. This dampened anti-metastatic effect may reflect the more potent impact of stable SLC7A11 knockdown from tumour establishment. However, the overall lower frequency of metastases in our therapeutic model (due to biological variation), may have limited statistical power. Future studies will assess this in more metastatic models of the disease. We also observed decreased CAF activation and intratumoural collagen (fibrosis), as well as normalised tumour vasculature. It should be noted that our approach used human-specific SLC7A11-siRNA and would not have targeted mouse cells. Thus, observed effects may be an underestimate as mouse CAFs can be co-recruited/activated in the model. Regardless, our results

Downloaded from cancerres.aacrjournals.org on July 31, 2021. © 2021 American Association for Cancer Research.

Author Manuscript Published OnlineFirst on May 12, 2021; DOI: 10.1158/0008-5472.CAN-20-2496
Author manuscripts have been peer reviewed and accepted for publication but have not yet been edited.

demonstrate the efficacy of Star 3+SLC7A11-siRNA against PDAC tumours and its potential to alleviate a drug delivery barrier. While we did not sensitise tumours to Abraxane® in our study, the dosing schedule selected was suboptimal to test whether SLC7A11 inhibition could sensitise to lower amounts of Abraxane®. Future studies will investigate chemosensitisation to higher doses of Abraxane and other potential therapeutic combinations that increase oxidative stress.

There is also some debate around the role of fibrosis in PDAC progression, with some studies in transgenic mouse PDAC models suggesting the PDAC stroma restrains tumour growth (55-57). Limitations of these studies included off-target effects on vasculature, causing hypoxia that drives more aggressive disease, and interference in signalling pathways that may have affected stromal cells that restrain tumour growth. Moreover, genetic ablation studies from tumour development may not reflect a late-stage tumour's response to therapeutic inhibition. However, these studies highlight the need to specifically target stromal cell populations that support tumour growth. Our approach overcomes these limitations by targeting a key metabolic function in both CAFs and PDAC cells, and reduces rather than depletes fibrosis and activated CAFs.

Finally, we validated our *in vivo* findings using PDAC patient-derived 3D explant model developed by our lab that retains the extensive fibrosis, 3D spatial architecture and cellular/stromal interactions of the original patient's tumour (46). In multiple patient explants, SLC7A11 inhibition or knockdown significantly reduced tumour cell and activated CAF frequency, confirming our *in vitro* and *in vivo* findings. This study brings together over a decade of research into the therapeutic potential of SLC7A11 inhibition in PDAC. Taken together, our findings and those of previous studies have demonstrated that SLC7A11 inhibition in PDAC is a multi-pronged therapeutic approach that targets both tumour and stroma to exert its maximal therapeutic effect.

Data Availability

All data generated or analysed during this study are included in this published article (and its Supplementary Information) and can be made available upon reasonable request. Expression array data for the PACA-AU cohort is publicly available through the ICGC data portal (*https://dcc.icgc.org/projects/PACA-AU*). More specific PDAC patient cohort data can be

Downloaded from cancerres.aacrjournals.org on July 31, 2021. © 2021 American Association for Cancer Research.

Author Manuscript Published OnlineFirst on May 12, 2021; DOI: 10.1158/0008-5472.CAN-20-2496
Author manuscripts have been peer reviewed and accepted for publication but have not yet been edited.

obtained through the Australian Pancreatic Cancer Genome Initiative. We are willing to share CAF cells, which would require appropriate human ethics approvals and an MTA with our laboratory.

AUTHOR CONTRIBUTIONS

GS, JM and AA share an equal author position. The order of equal authors was based on relative contribution of the co-first authors to experimental design, analysis of results and composition of the manuscript. GS, JM and PP led the project, designed/performed the majority of experiments, interpreted data, and wrote the manuscript. GS, JM, PP, AA, CK, JY, RMCI, SN, JL, NR, JL, EG-A, JK performed in vitro and in vivo orthotopic tumour experiments. MP, BJM provided TKCC5 cells and intellectual guidance on their use. JK, JK performed explant experiments and analysis. GS, JY, JK performed sub-cutaneous and orthotopic (stable line) mouse models. JH performed cystine uptake assays. YFG performed metabolic profiling. JH and NT provided intellectual guidance on interpretation of metabolism-related results. CB and TPD synthesised and characterised Star 3 nanoparticles. ME isolated CAFs and MA isolated PSCs used in this study. PT, TRC, BAP, JLC and YS performed in vitro collagen plug assays and collagen analysis. SF, AKN, ADC, and OJS performed transgenic mouse experiments. DG, AC, AJ, AG and KH provided guidance on SLC7A11 scoring and analysis in the PDAC patient cohort study. VG performed statistical analyses for the PDAC patient cohort study. JPM provided guidance on all in vivo aspects of the study. All authors reviewed the manuscript. We also acknowledge the contribution of the Australian Pancreatic Cancer Genome Initiative in providing the valuable PDAC patient specimens and survival data utilised in the PDAC patient cohort study. **Australian Pancreatic Cancer Genome Initiative (APGI): Garvan Institute of Medical Research** Amber L. Johns[1], Anthony J Gill[1, 5], David K. Chang[1, 22], Lorraine A. Chantrill[1,8], Angela Chou[1,5], Marina Pajic[1], Angela Steinmann[1], Mehreen Arshi[1], Ali Drury[1], Danielle Froio[1], Ashleigh Parkin[1], Paul Timpson[1], David Hermann[1]. **QIMR Berghofer Medical Research Institute** Nicola Waddell[2], John V. Pearson[2], Ann-Marie Patch[2], Katia Nones[2], Felicity Newell[2], Pamela Mukhopadhyay[2], Venkateswar Addala[2], Stephen Kazakoff[2], Oliver Holmes[2], Conrad Leonard[2], Scott Wood[2], Christina Xu[2]. **University of Melbourne, Centre for Cancer Research** Sean M. Grimmond[3], Oliver Hofmann[3]. **University of QLD, IMB** Angelika Christ[4], Tim Bruxner[4]. **Royal North Shore Hospital** Jaswinder S. Samra[5], Jennifer Arena[5], Nick Pavlakis[5,] Hilda A.

Downloaded from cancerres.aacrjournals.org on July 31, 2021. © 2021 American Association for Cancer Research.

Author Manuscript Published OnlineFirst on May 12, 2021; DOI: 10.1158/0008-5472.CAN-20-2496
Author manuscripts have been peer reviewed and accepted for publication but have not yet been edited.

High[5], Anubhav Mittal[5]. **Bankstown Hospital** Ray Asghari[6], Neil D. Merrett[6], Darren Pavey[6], Amitabha Das[6]. **Liverpool Hospital** Peter H. Cosman[7], Kasim Ismail[7], Chelsie O'Connnor[7]. **St Vincent's Hospital** Alina Stoita[8], David Williams[8], Allan Spigellman[8]**. Westmead Hospital** Vincent W. Lam[9,] Duncan McLeod[9], Adnan M. Nagrial[1,9], Judy Kirk[9]. **Royal Prince Alfred Hospital, Chris O'Brien Lifehouse** James G. Kench[10], Peter Grimison[10], Caroline L. Cooper[10], Charbel Sandroussi[10], Annabel Goodwin[7,10]. **Prince of Wales Hospital** R. Scott Mead[1,11], Katherine Tucker[11], Lesley Andrews[11]. **Fremantle Hospital** Michael Texler[12], Cindy Forest[12], Krishna P. Epari[12], Mo Ballal[12], David R. Fletcher[12], Sanjay Mukhedkar[12]. **St John of God Healthcare** Nikolajs Zeps[14], Maria Beilin[14], Kynan Feeney[14]. **Royal Adelaide Hospital** Nan Q Nguyen[15], Andrew R. Ruszkiewicz[15], Chris Worthley[15]. **Flinders Medical Centre** John Chen[16], Mark E. Brooke-Smith[16], Virginia Papangelis[16]. **Envoi Pathology** Andrew D. Clouston[17], Patrick Martin[17]. **Princess Alexandria Hospital** Andrew P. Barbour[18], Thomas J. O'Rourke[18], Jonathan W. Fawcett[18], Kellee Slater[18], Michael Hatzifotis[18], Peter Hodgkinson[18]. **Austin Hospital** Mehrdad Nikfarjam[19]. **Johns Hopkins Medical Institutes** James R. Eshleman[20], Ralph H. Hruban[20], Christopher L. Wolfgang[20], Mary Hodgin[20]. **ARC-Net Centre for Applied Research on Cancer** Aldo Scarpa[21], Rita T. Lawlor[21], Stefania Beghelli[21], Vincenzo Corbo[21], Maria Scardoni[21], Claudio Bassi[21]. **University of Glasgow** Andrew V Biankin[1, 22], Judith Dixon[22], Craig Nourse[22], Nigel B. Jamieson[22]. [1]The Kinghorn Cancer Centre, Garvan Institute of Medical Research, 370 Victoria Street, Darlinghurst, Sydney, New South Wales 2010, Australia. [2]QIMR Berghofer Medical Research Institute, 300 Herston Rd, Herston, Queensland 4006, Australia. [3]University of Melbourne, Centre for Cancer Research, Victorian Comprehensive Cancer Centre, 305 Grattan Street, Melbourne, Victoria 3000, Australia. [4] Institute for Molecular Bioscience, University of QLD, St Lucia, Queensland 4072, Australia. [5]Royal North Shore Hospital, Westbourne Street, St Leonards, New South Wales 2065, Australia. [6]Bankstown Hospital, Eldridge Road, Bankstown, New South Wales 2200, Australia. [7]Liverpool Hospital, Elizabeth Street, Liverpool, New South Wales 2170, Australia. [8] St Vincent's Hospital, 390 Victoria Street, Darlinghurst, New South Wales, 2010 Australia. [9]Westmead Hospital, Hawkesbury and Darcy Roads, Westmead, New South Wales 2145, Australia. [10]Royal Prince Alfred Hospital, Missenden Road, Camperdown, New South Wales 2050, Australia. [11]Prince of Wales Hospital, Barker Street, Randwick, New South Wales 2031, Australia. [12]Fremantle Hospital, Alma Street, Fremantle, Western Australia 6959, Australia. [13]Sir Charles Gairdner

Downloaded from cancerres.aacrjournals.org on July 31, 2021. © 2021 American Association for Cancer Research.

Author Manuscript Published OnlineFirst on May 12, 2021; DOI: 10.1158/0008-5472.CAN-20-2496
Author manuscripts have been peer reviewed and accepted for publication but have not yet been edited.

Hospital, Hospital Avenue, Nedlands, Western Australia 6009, Australia. [14]St John of God Healthcare, 12 Salvado Road, Subiaco, Western Australia 6008, Australia. [15]Royal Adelaide Hospital, North Terrace, Adelaide, South Australia 5000, Australia. [16]Flinders Medical Centre, Flinders Drive, Bedford Park, South Australia 5042, Australia. [17]Envoi Pathology, 1/49 Butterfield Street, Herston, Queensland 4006, Australia. [18]Princess Alexandria Hospital, Cornwall Street & Ipswich Road, Woolloongabba, Queensland 4102, Australia. [19]Austin Hospital, 145 Studley Road, Heidelberg, Victoria 3084, Australia. [20]Johns Hopkins Medical Institute, 600 North Wolfe Street, Baltimore, Maryland 21287, USA. [21]ARC-NET Center for Applied Research on Cancer, University of Verona, Via dell'Artigliere, 19 37129 Verona, Province of Verona, Italy. [22]Wolfson Wohl Cancer Research Centre, Institute of Cancer Sciences, University of Glasgow, Garscube Estate, Switchback Road, Bearsden, Glasgow, Scotland G61 1BD, United Kingdom). All authors have reviewed and approved this manuscript.

ACKNOWLEDGEMENTS

We would like to thank Dr Andrea Nunez and Ms Amanda Mawson for their assistance in mouse monitoring. We acknowledge the Flow Cytometry, Biomedical Imaging, and Biological Resource Imaging Facilities within the Mark Wainwright Analytical Centre at the University of New South Wales for their technical support. Biospecimens and clinical data for prognostic studies were provided by the APGI (www.pancreaticcancer.net.au) which is supported by an Avner Grant from PanKind, The Australian Pancreatic Cancer Foundation (www.pankind.org.au). Biospecimens and data used for 3D explants were obtained from the HSA Biobank, UNSW Biorepository, UNSW Sydney, Australia. We sincerely thank the patients who consented to donate their tumour samples for research. We would like to thank Dr Carmel Quinn and Dr Anusha Hettiaratchi of the HSA Biobank for their support in managing clinical samples and patient consent. We would also like to acknowledge our community consumers Mr Gino Iori and Ms Claire Harvey for their invaluable input on the project and grant applications. **Financial support:** This research was made possible by major funding from NHMRC project grant (P.A. Phillips, J.A. McCarroll, J.P. Morton, D. Goldstein, APP1144108) and an Avner Grant from PanKind, The Australian Pancreatic Cancer Foundation (Avner Innovation Grant [P.A. Phillips, J.A. McCarroll, D. Goldstein, J. Holst, J.P. Morton, T.P. Davis and G. Sharbeen,

Downloaded from cancerres.aacrjournals.org on July 31, 2021. © 2021 American Association for Cancer Research.

Author Manuscript Published OnlineFirst on May 12, 2021; DOI: 10.1158/0008-5472.CAN-20-2496
Author manuscripts have been peer reviewed and accepted for publication but have not yet been edited.

APCF0050618]; www.avnersfoundation.org.au). The following sources supported author contributions and research: NHMRC CDF-I (P.A. Phillips, APP1024896), Cancer-Institute NSW ECF/CDFs (P.A. Phillips 08/ECF/1-37; G. Sharbeen, CDF181166; J.A. McCarroll, CDF102; T.R. Cox, CDF171105), Cancer Institute NSW Innovation Grant (P.A. Phillips, 09/RFG/2-58), Cancer Institute NSW 'The Professor Rob Sutherland AO Make a Difference Award' (D. Goldstein, 2017/AWD002), Cancer Australia/Cancer Council (P.A. Phillips, J.A. McCarroll and D. Goldstein, APP1126736), Cancer Australia/Kids Cancer Project (APP1184840, J.A. McCarroll, P.A. Phillips, T.P. Davis), Translational Cancer Research Network and Australian Postgraduate Award Scholarships (A. Akerman), Australian Government Research Training Program Scholarship & UNSW Sydney Scientia PhD Scholarship (J. Kokkinos), Cure Cancer Australia (G. Sharbeen, APP1122758), Tour de Cure PhD Support Scholarship (J. Kokkinos, P.A. Phillips, D. Goldstein, RSP-011-18/19), Tour de Cure Established Research Grant (P.A. Phillips, J.A. McCarroll, D. Goldstein, UNSWR002; RSP-235-19/20), Tour de Cure Pioneering Research Grant (G. Sharbeen, P.A. Phillips, D. Goldstein UNSWR004; RSP-255-19/20), Cancer Research UK Core Funding and Grand Challenge grants (O.J. Sansom, A.D. Campbell, A.K. Najumudeen and S.K. Fey, A17196, A21139, A25045), Pancreatic Cancer UK Future Leaders Academy (O.J. Sansom, S.K. Fey), NHRMC project grants (T.R. Cox and J.L. Chitty, APP1140125), NHMRC CDF-II (T.R. Cox, APP1158590), NHMRC Senior Research Fellowship (P. Timpson, APP1136974), Len Ainsworth Pancreatic Cancer Fellowship and support from Suttons, Cancer Council NSW (T.R. Cox and J.L. Chitty, RG19-09). We also acknowledge the generous philanthropic support of Mr Paul Dainty, Dr Marjorie O'Neil and Dr Keri Spooner.

REFERENCES

1. Siegel RL, Miller KD, Jemal A. Cancer statistics, 2019. CA Cancer J Clin **2019**;69:7-34
2. McCarroll JA, Naim S, Sharbeen G, Russia N, Lee J, Kavallaris M, *et al.* Role of pancreatic stellate cells in chemoresistance in pancreatic cancer. Front Physiol **2014**;5:141
3. Murakami T, Hiroshima Y, Matsuyama R, Homma Y, Hoffman RM, Endo I. Role of the tumor microenvironment in pancreatic cancer. Ann Gastroenterol Surg **2019**;3:130-7

Downloaded from cancerres.aacrjournals.org on July 31, 2021. © 2021 American Association for Cancer Research.

Author Manuscript Published OnlineFirst on May 12, 2021; DOI: 10.1158/0008-5472.CAN-20-2496
Author manuscripts have been peer reviewed and accepted for publication but have not yet been edited.

4. Pereira BA, Vennin C, Papanicolaou M, Chambers CR, Herrmann D, Morton JP, *et al.* CAF Subpopulations: A New Reservoir of Stromal Targets in Pancreatic Cancer. Trends Cancer **2019**;5:724-41
5. Vaziri-Gohar A, Zarei M, Brody JR, Winter JM. Metabolic Dependencies in Pancreatic Cancer. Front Oncol **2018**;8:617
6. Sato H, Shiiya A, Kimata M, Maebara K, Tamba M, Sakakura Y, *et al.* Redox imbalance in cystine/glutamate transporter-deficient mice. The Journal of biological chemistry **2005**;280:37423-9
7. Sato H, Tamba M, Ishii T, Bannai S. Cloning and expression of a plasma membrane cystine/glutamate exchange transporter composed of two distinct proteins. The Journal of biological chemistry **1999**;274:11455-8
8. Sato H, Tamba M, Kuriyama-Matsumura K, Okuno S, Bannai S. Molecular cloning and expression of human xCT, the light chain of amino acid transport system xc. Antioxid Redox Signal **2000**;2:665-71
9. Banjac A, Perisic T, Sato H, Seiler A, Bannai S, Weiss N, *et al.* The cystine/cysteine cycle: a redox cycle regulating susceptibility versus resistance to cell death. Oncogene **2008**;27:1618-28
10. Wang K, Jiang J, Lei Y, Zhou S, Wei Y, Huang C. Targeting Metabolic-Redox Circuits for Cancer Therapy. Trends Biochem Sci **2019**;44:401-14
11. Chen RS, Song YM, Zhou ZY, Tong T, Li Y, Fu M, *et al.* Disruption of xCT inhibits cancer cell metastasis via the caveolin-1/beta-catenin pathway. Oncogene **2009**;28:599-609
12. Gout PW, Buckley AR, Simms CR, Bruchovsky N. Sulfasalazine, a potent suppressor of lymphoma growth by inhibition of the x(c)- cystine transporter: A new action for an old drug. Leukemia **2001**;15:1633-40
13. Guan J, Lo M, Dockery P, Mahon S, Karp CM, Buckley AR, *et al.* The xc- cystine/glutamate antiporter as a potential therapeutic target for small-cell lung cancer: use of sulfasalazine. Cancer Chemother Pharmacol **2009**;64:463-72
14. Huang Y, Dai Z, Barbacioru C, Sadee W. Cystine-glutamate transporter SLC7A11 in cancer chemosensitivity and chemoresistance. Cancer Res **2005**;65:7446-54
15. Ji X, Qian J, Rahman SMJ, Siska PJ, Zou Y, Harris BK, *et al.* xCT (SLC7A11)-mediated metabolic reprogramming promotes non-small cell lung cancer progression. Oncogene **2018**;37:5007-19
16. Lyons SA, Chung WJ, Weaver AK, Ogunrinu T, Sontheimer H. Autocrine glutamate signaling promotes glioma cell invasion. Cancer Res **2007**;67:9463-71
17. Lo M, Ling V, Wang YZ, Gout PW. The xc- cystine/glutamate antiporter: A mediator of pancreatic cancer growth with a role in drug resistance. British journal of cancer **2008**;99:464-72
18. Lo M, Ling V, Low C, Wang YZ, Gout PW. Potential use of the anti-inflammatory drug, sulfasalazine, for targeted therapy of pancreatic cancer. Current oncology **2010**;17:9-16
19. Mukhopadhyay S, Biancur DE, Parker SJ, Yamamoto K, Banh RS, Paulo JA, *et al.* Autophagy is required for proper cysteine homeostasis in pancreatic cancer through regulation of SLC7A11. Proc Natl Acad Sci U S A **2021**;118
20. Arensman MD, Yang XS, Leahy DM, Toral-Barza L, Mileski M, Rosfjord EC, *et al.* Cystine-glutamate antiporter xCT deficiency suppresses tumor growth while preserving antitumor immunity. Proc Natl Acad Sci U S A **2019**;116:9533-42

Downloaded from cancerres.aacrjournals.org on July 31, 2021. © 2021 American Association for Cancer Research.

Author Manuscript Published OnlineFirst on May 12, 2021; DOI: 10.1158/0008-5472.CAN-20-2496
Author manuscripts have been peer reviewed and accepted for publication but have not yet been edited.

21. Daher B, Parks SK, Durivault J, Cormerais Y, Baidarjad H, Tambutte E, *et al.* Genetic ablation of the cystine transporter xCT in PDAC cells inhibits mTORC1, growth, survival and tumor formation via nutrient and oxidative stresses. Cancer Res **2019**
22. Ohman KA, Hashim YM, Vangveravong S, Nywening TM, Cullinan DR, Goedegebuure SP, *et al.* Conjugation to the sigma-2 ligand SV119 overcomes uptake blockade and converts dm-Erastin into a potent pancreatic cancer therapeutic. Oncotarget **2016**;7:33529-41
23. Badgley MA, Kremer DM, Maurer HC, DelGiorno KE, Lee HJ, Purohit V, *et al.* Cysteine depletion induces pancreatic tumor ferroptosis in mice. Science **2020**;368:85-9
24. Kshattry S, Saha A, Gries P, Tiziani S, Stone E, Georgiou G, *et al.* Enzyme-mediated depletion of l-cyst(e)ine synergizes with thioredoxin reductase inhibition for suppression of pancreatic tumor growth. NPJ Precis Oncol **2019**;3:16
25. Sousa CM, Biancur DE, Wang X, Halbrook CJ, Sherman MH, Zhang L, *et al.* Pancreatic stellate cells support tumour metabolism through autophagic alanine secretion. Nature **2016**;536:479-83
26. Zhang W, Trachootham D, Liu J, Chen G, Pelicano H, Garcia-Prieto C, *et al.* Stromal control of cystine metabolism promotes cancer cell survival in chronic lymphocytic leukaemia. Nat Cell Biol **2012**;14:276-86
27. McCarroll JA, Sharbeen G, Liu J, Youkhana J, Goldstein D, McCarthy N, *et al.* betaIII-tubulin: a novel mediator of chemoresistance and metastases in pancreatic cancer. Oncotarget **2015**;6:2235-49
28. Sharbeen G, McCarroll J, Liu J, Youkhana J, Limbri LF, Biankin AV, *et al.* Delineating the Role of betaIV-Tubulins in Pancreatic Cancer: betaIVb-Tubulin Inhibition Sensitizes Pancreatic Cancer Cells to Vinca Alkaloids. Neoplasia **2016**;18:753-64
29. Sharbeen G, Youkhana J, Mawson A, McCarroll J, Nunez A, Biankin A, *et al.* MutY-Homolog (MYH) inhibition reduces pancreatic cancer cell growth and increases chemosensitivity. Oncotarget **2017**;8:9216-29
30. Chou A, Froio D, Nagrial AM, Parkin A, Murphy KJ, Chin VT, *et al.* Tailored first-line and second-line CDK4-targeting treatment combinations in mouse models of pancreatic cancer. Gut **2018**;67:2142-55
31. Ouyang H, Mou L, Luk C, Liu N, Karaskova J, Squire J, *et al.* Immortal human pancreatic duct epithelial cell lines with near normal genotype and phenotype. Am J Pathol **2000**;157:1623-31
32. Apte MV, Haber PS, Applegate TL, Norton ID, McCaughan GW, Korsten MA, *et al.* Periacinar stellate shaped cells in rat pancreas: identification, isolation, and culture. Gut **1998**;43:128-33
33. Bachem MG, Schneider E, Gross H, Weidenbach H, Schmid RM, Menke A, *et al.* Identification, culture, and characterization of pancreatic stellate cells in rats and humans. Gastroenterology **1998**;115:421-32
34. Vonlaufen A, Joshi S, Qu C, Phillips PA, Xu Z, Parker NR, *et al.* Pancreatic stellate cells: Partners in crime with pancreatic cancer cells. Cancer Res **2008**;68:2085-93
35. Morton JP, Timpson P, Karim SA, Ridgway RA, Athineos D, Doyle B, *et al.* Mutant p53 drives metastasis and overcomes growth arrest/senescence in pancreatic cancer. Proc Natl Acad Sci U S A **2010**;107:246-51
36. Edfors F, Hober A, Linderback K, Maddalo G, Azimi A, Sivertsson A, *et al.* Enhanced validation of antibodies for research applications. Nat Commun **2018**;9:4130

Downloaded from cancerres.aacrjournals.org on July 31, 2021. © 2021 American Association for Cancer Research.

Author Manuscript Published OnlineFirst on May 12, 2021; DOI: 10.1158/0008-5472.CAN-20-2496
Author manuscripts have been peer reviewed and accepted for publication but have not yet been edited.

37. Ohlund D, Handly-Santana A, Biffi G, Elyada E, Almeida AS, Ponz-Sarvise M, *et al.* Distinct populations of inflammatory fibroblasts and myofibroblasts in pancreatic cancer. J Exp Med **2017**;214:579-96
38. Wang Q, Hardie RA, Hoy AJ, van Geldermalsen M, Gao D, Fazli L, *et al.* Targeting ASCT2-mediated glutamine uptake blocks prostate cancer growth and tumour development. J Pathol **2015**;236:278-89
39. Mackay GM, Zheng L, van den Broek NJ, Gottlieb E. Analysis of Cell Metabolism Using LC-MS and Isotope Tracers. Methods Enzymol **2015**;561:171-96
40. Conway JRW, Vennin C, Cazet AS, Herrmann D, Murphy KJ, Warren SC, *et al.* Three-dimensional organotypic matrices from alternative collagen sources as pre-clinical models for cell biology. Sci Rep **2017**;7:16887
41. Vennin C, Melenec P, Rouet R, Nobis M, Cazet AS, Murphy KJ, *et al.* CAF hierarchy driven by pancreatic cancer cell p53-status creates a pro-metastatic and chemoresistant environment via perlecan. Nat Commun **2019**;10:3637
42. Hingorani SR, Wang L, Multani AS, Combs C, Deramaudt TB, Hruban RH, *et al.* Trp53R172H and KrasG12D cooperate to promote chromosomal instability and widely metastatic pancreatic ductal adenocarcinoma in mice. Cancer Cell **2005**;7:469-83
43. Teo J, McCarroll JA, Boyer C, Youkhana J, Sagnella SM, Duong HT, *et al.* A Rationally Optimized Nanoparticle System for the Delivery of RNA Interference Therapeutics into Pancreatic Tumors in Vivo. Biomacromolecules **2016**;17:2337-51
44. Cazet AS, Hui MN, Elsworth BL, Wu SZ, Roden D, Chan CL, *et al.* Targeting stromal remodeling and cancer stem cell plasticity overcomes chemoresistance in triple negative breast cancer. Nat Commun **2018**;9:2897
45. Ishii T, Bannai S, Sugita Y. Mechanism of growth stimulation of L1210 cells by 2-mercaptoethanol in vitro. Role of the mixed disulfide of 2-mercaptoethanol and cysteine. The Journal of biological chemistry **1981**;256:12387-92
46. Kokkinos J, Sharbeen G, Haghighi KS, Ignacio RMC, Kopecky C, Gonzales-Aloy E, *et al.* Ex vivo culture of intact human patient derived pancreatic tumour tissue. Sci Rep **2021**;11:1944
47. Bailey P, Chang DK, Nones K, Johns AL, Patch AM, Gingras MC, *et al.* Genomic analyses identify molecular subtypes of pancreatic cancer. Nature **2016**;531:47-52
48. Zhu S, Zhang Q, Sun X, Zeh HJ, 3rd, Lotze MT, Kang R, *et al.* HSPA5 Regulates Ferroptotic Cell Death in Cancer Cells. Cancer Res **2017**;77:2064-77
49. Ma Z, Zhang H, Lian M, Yue C, Dong G, Jin Y, *et al.* SLC7A11, a component of cysteine/glutamate transporter, is a novel biomarker for the diagnosis and prognosis in laryngeal squamous cell carcinoma. Oncol Rep **2017**;38:3019-29
50. Zhang L, Huang Y, Ling J, Zhuo W, Yu Z, Luo Y, *et al.* Overexpression of SLC7A11: a novel oncogene and an indicator of unfavorable prognosis for liver carcinoma. Future Oncol **2018**;14:927-36
51. Maurer C, Holmstrom SR, He J, Laise P, Su T, Ahmed A, *et al.* Experimental microdissection enables functional harmonisation of pancreatic cancer subtypes. Gut **2019**;68:1034-43
52. Alonso V, Linares V, Belles M, Albina ML, Sirvent JJ, Domingo JL, *et al.* Sulfasalazine induced oxidative stress: a possible mechanism of male infertility. Reprod Toxicol **2009**;27:35-40

Downloaded from cancerres.aacrjournals.org on July 31, 2021. © 2021 American Association for Cancer Research.

Author Manuscript Published OnlineFirst on May 12, 2021; DOI: 10.1158/0008-5472.CAN-20-2496
Author manuscripts have been peer reviewed and accepted for publication but have not yet been edited.

53. Wahl C, Liptay S, Adler G, Schmid RM. Sulfasalazine: a potent and specific inhibitor of nuclear factor kappa B. J Clin Invest **1998**;101:1163-74
54. Weber CK, Liptay S, Wirth T, Adler G, Schmid RM. Suppression of NF-kappaB activity by sulfasalazine is mediated by direct inhibition of IkappaB kinases alpha and beta. Gastroenterology **2000**;119:1209-18
55. Lee JJ, Perera RM, Wang H, Wu DC, Liu XS, Han S, *et al.* Stromal response to Hedgehog signaling restrains pancreatic cancer progression. Proc Natl Acad Sci U S A **2014**;111:E3091-100
56. Ozdemir BC, Pentcheva-Hoang T, Carstens JL, Zheng X, Wu CC, Simpson TR, *et al.* Depletion of carcinoma-associated fibroblasts and fibrosis induces immunosuppression and accelerates pancreas cancer with reduced survival. Cancer Cell **2014**;25:719-34
57. Rhim AD, Oberstein PE, Thomas DH, Mirek ET, Palermo CF, Sastra SA, *et al.* Stromal elements act to restrain, rather than support, pancreatic ductal adenocarcinoma. Cancer Cell **2014**;25:735-47

FIGURE LEGENDS

Figure 1: SLC7A11 is upregulated in human CAFs and predicts poorer overall survival in human PDAC patients. A) Quantitative real-time PCR analysis (mean+s.e.m.) of SLC7A11 and SLC3A2 expression in RNA extracts from normal pancreatic fibroblasts (n=8 patients with benign pancreatic conditions) and patient-derived CAFs (n=10 PDAC patients). Circles = independent patients (*p≤0.05, student t-test). B) Western blot of SLC7A11 in protein extracts from human PDAC cells and CAFs (n=6 patients). α-tubulin = loading control. C) Immunofluorescence for DAPI, αSMA and SLC7A11 in a human PDAC tissue specimen obtained through the APGI. (D-G) Human PDAC tissue microarrays (APGI International Cancer Genome Consortium cohort) were stained for SLC7A11. D) Samples selected as score references (insets show magnified view). Scores of 0-1 = SLC7A11 low ($Tumour^{low}$, $Stroma^{low}$), scores of 2-3 = SLC7A11 high ($Tumour^{high}$, $Stroma^{high}$). Dashed lines delineate tumour and stroma. E-G)

Downloaded from cancerres.aacrjournals.org on July 31, 2021. © 2021 American Association for Cancer Research.

Author Manuscript Published OnlineFirst on May 12, 2021; DOI: 10.1158/0008-5472.CAN-20-2496
Author manuscripts have been peer reviewed and accepted for publication but have not yet been edited.

Kaplan-Meier survival curves showing the correlation between SLC7A11 expression in tumour cells (E), stroma (F), or both (G) with overall patient survival (days post-diagnosis). Total patient numbers per group are indicated in keys. Asterisks indicate significance based on (F) multivariate analysis (G) Log-Rank test (*p≤0.05). H) Representative photos of combined tumour and stroma score groups. Scale bars in all photos = 100µm.

Figure 2: SLC7A11 inhibition in CAFs reduced proliferation and antioxidant capacity by inhibiting cystine uptake and glutathione production and inducing senescence. A) Cell proliferation (cell counting kit 8) of CAFs 72h post-transfection with non-silencing siRNA (ns-siRNA) or SLC7A11-siRNA pool (n=6). B) Cell proliferation of CAFs treated with sulfasalazine (SSZ) ± 66µM 2-mercaptoethanol (2-ME) (n=3). C) Live CAF counts post-treatment with erastin. (n=4). D-E) Radiolabelled cystine uptake (n=3). F-G) Intracellular glutathione levels by colorimetric assay (n=3). H-I) Intracellular oxidative stress with or without tert-butyl hydroperoxide (tBHP; oxidative stress), based on CellROX staining (percent of 0µM tBHP controls; n=3). J) Live CAF counts 72h post-transfection with ns-siRNA, SLC7A11-siRNA pool or SLC7A11-siRNA single sequence (SLC7A11-siRNA single seq) and 24h post-tBHP (n=4). K) Frequency of AnnexinV+DAPI positive (apoptotic) cells, (percent of 0µM tBHP controls), 72h post-transfection and 24h post-tBHP. L) Glutathione peroxidase activity of CAFs treated with erastin (n=4). M) Live CAF counts post-treatment with 40µM erastin ± 2µM ferrostatin (n=4). N) Live cell counts of immortalised CAFs expressing scramble-shRNA or SLC7A11-shRNA, 72h post-seeding and 24h post-tBHP. (n=3). O) As per L, except immortalised CAFs stably expressing shRNA were used and treated with 40µM tBHP, instead of erastin (n=3). P-Q) β-galactosidase positive (senescent) CAFs as a fraction of total CAFs: (P) 72h post-transfection with ns-siRNA or SLC7A11-siRNA or (Q) 48h post-treatment with SSZ. Circles in graphs indicate replicates, lines and bars represent mean±s.e.m. All data in panels A-O are expressed as percent of controls. Asterisks and hashes in all graphs indicate significance (ns=not significant, *p≤0.05, **p≤0.01, ***p≤0.001, ****p≤0.0001 # p≤0.05, ## p≤0.01, relative to ns-siRNA at same tBHP concentration). Panels (A,C-E,L,P-Q) = student t-test. Panels (B,F-K,M-O) = One-way ANOVA. Replicate numbers in (A-M, P-Q) refer to experiments performed using independent primary CAF cells isolated from different PDAC patients. Replicate numbers in (N-O) refer to repeated experiments using hTERT-immortalised CAFs.

Downloaded from cancerres.aacrjournals.org on July 31, 2021. © 2021 American Association for Cancer Research.

Author Manuscript Published OnlineFirst on May 12, 2021; DOI: 10.1158/0008-5472.CAN-20-2496
Author manuscripts have been peer reviewed and accepted for publication but have not yet been edited.

Figure 3: SLC7A11 knockdown in CAFs reduced PDAC 3D co-culture spheroid growth and collagen remodelling *in vitro*. A-B) Schematic diagrams of 3D co-culture spheroid outgrowth assay (A), and growth assay (B). C) Quantification of spheroid outgrowth post-transfection with control-siRNA (ns-siRNA) or SLC7A11-siRNA pool. Labels: $MiaPaCa2_{ns\text{-}siRNA}$, $CAF_{ns\text{-}siRNA}$ = controls; $MiaPaCa2_{slc\text{-}siRNA}$, $CAF_{slc\text{-}siRNA}$ = SLC7A11 knockdown. Representative photos are shown above each bar with the core in white lines and outgrowth in red lines (n=3; scale bars = 300µm). D) Representative photos (scale bars = 200µm) and quantification of spheroid growth. Labels: $MiaPaCa2_{ctl\text{-}shRNA}$, $CAF_{ctl\text{-}shRNA}$ = scramble-shRNA controls; $PDAC_{slc\text{-}shRNA}$, $CAF_{slc\text{-}shRNA}$ = SLC7A11-shRNA. E-G) (E) TKCC5, (F) Panc1 and (G) AsPC1 PDAC cells were co-cultured with $CAF_{ctl\text{-}shRNA}$ or $CAF_{slc\text{-}shRNA}$ cells as in (D). Line graphs show spheroid cross-section area based on daily bright field microscope photos, as a percent of day 0 (n=3-6). H) Schematic diagram of assay and representative photos of collagen plugs contracted by siRNA-transfected CAFs. Line graph shows the average area of plugs over time (n=4). I-L) Representative images and analysis of collagen content in plugs at endpoint (n=4). I) Average picrosirius red signal. J) Average total birefringence. K) Average % of total birefringence that was high (red-orange), medium (yellow) and low (green). L) Top graph shows the average maximum second harmonics generation (SHG) signal. Bottom graph shows average correlation based on GLCM analysis of SHG maximum intensity projections. Circles in graphs indicate replicates, lines and bars in all graphs represent mean±s.e.m. Asterisks in graphs indicate significance (ns=not significant, *p≤0.05, **p≤0.01, ***p≤0.001). Panels (E-L) = student t-test. Panels (C-D) = One-way ANOVA. Replicate numbers in (C, H-L) refer to experiments performed using independent primary CAFs from different PDAC patients. Replicate numbers in (D-G) refer to repeated experiments using immortalised CAFs.

Figure 4: Genetic ablation of SLC7A11 in PDAC cells had no effect on pancreatic tumour growth *in vivo*. A) In situ hybridisation for SLC7A11 transcripts in KPC and KPC *slc7a11*$^{fl/fl}$ tumour sections. Red = SLC7A11 signal. B) Western blot for SLC7A11 in protein extracts from KPC and KPC *slc7a11*$^{fl/fl}$ mice. Graph shows densitometry for SLC7A11, standardised to HSP90 (n=4). Scale bars = 20µm. C) Quantification of Pancreatic Intraepithelial Neoplasia (PanINs) 1A-3 from KC mice (n=7) and KC mice with conditional SLC7A11 KO under *Pdx1*-promoter (KC *Slc7a11*$^{fl/fl}$; n=7) at 70 days of age. D) Kaplan-Meier analysis showing survival percentage of KPC (n=26) and KPC *Slc7a11*$^{fl/fl}$ mice (n=24) mice. E-F) Representative photos of KPC and

Downloaded from cancerres.aacrjournals.org on July 31, 2021. © 2021 American Association for Cancer Research.

Author Manuscript Published OnlineFirst on May 12, 2021; DOI: 10.1158/0008-5472.CAN-20-2496
Author manuscripts have been peer reviewed and accepted for publication but have not yet been edited.

KPC *Slc7a11*$^{fl/fl}$ tumour sections probed for (E) αSMA (brown) and (F) picrosirius red (collagen). Scale bars = 400μm. Bar graphs show quantification of (E) αSMA staining and (F) picrosirius red staining (n=5 mice/group). G-H) Live cell counts of (G) KPC PDAC cells and (H) KPC CAFs 72h post-transfection with control-siRNA (ns-siRNA) or mouse SLC7A11-siRNA pool (SLC7A11 pool; n=3). Panels (B-C, E-F): Circles indicate replicates, lines represent mean±s.e.m. Asterisks indicate significance (*p≤0.05, ***p≤0.010). Panels B, E-H= student t-test. Panel C = One-way ANOVA.

Figure 5: SLC7A11 knockdown in CAFs reduced sub-cutaneous PDAC tumour incidence and knockdown in both PDAC cells and CAFs reduced orthotopic tumour growth, fibrosis and metastases. A) Sub-cutaneous tumours with co-injection of TKCC5 PDAC cells and immortalised CAFs expressing scramble-shRNA ($CAF_{ctl\text{-}shRNA}$) or SLC7A11-shRNA ($CAF_{slc\text{-}shRNA}$). Bar graph shows incidence of tumours at endpoint. B-D) MiaPaCa2 PDAC cells and immortalised CAF cells expressing scramble-shRNA ($MiaPaCa2_{ctl\text{-}shRNA}$, $CAF_{ctl\text{-}shRNA}$) or SLC7A11-shRNA ($MiaPaCa2_{slc\text{-}shRNA}$, $CAF_{slc\text{-}shRNA}$) were co-injected into the pancreas of host mice. Tumour growth was tracked by ultrasound. B) Line graphs show average tumour volumes over time. Symbols indicate mean±s.e.m. p-value is shown for endpoint (n=11-12; One-way ANOVA). C) Metastatic sites per mouse at endpoint, based on *ex vivo* luminescence (n=11-12). Representative H&E photos shown. Scale bars = 200μm. D) Representative photos of tumour sections probed with picrosirius red (collagen) and methyl green. Graph shows quantification of picrosirius red staining, based on Qupath analysis of representative regions (n=9-11). Scale bars = 50μm. Panels (C-D): lines = mean±s.e.m. Asterisks indicate significance (*p≤0.05, ** p≤0.01; One-way ANOVA). Symbols indicate individual mice.

Figure 6: Star 3+SLC7A11-siRNA treatment reduces orthotopic pancreatic tumour growth, intratumoural CAF activation and fibrosis, and normalised tumour vasculature. All orthotopic tumours were co-injections of PDAC cells and human primary patient-derived CAFs. A) Orthotopic tumours were treated with Star 3 nanoparticles + indicated siRNA in the regimen shown. Representative photos of SLC7A11 immunohistochemistry in tumour tissue are shown. Graph shows quantification of SLC7A11 staining intensity (optical density; n=3). B) Treatment regimen for therapeutic model in (C-D). C) Tumour volume at therapeutic model endpoint, as assessed by calliper measurement (n=7-8). D) Metastatic sites per mouse at model

Downloaded from cancerres.aacrjournals.org on July 31, 2021. © 2021 American Association for Cancer Research.

Author Manuscript Published OnlineFirst on May 12, 2021; DOI: 10.1158/0008-5472.CAN-20-2496
Author manuscripts have been peer reviewed and accepted for publication but have not yet been edited.

endpoint based on *ex vivo* luminescence imaging (n=7-8). Representative H&Es shown. E-F) Representative photos and quantification of (E) αSMA (brown) and (B) picrosirius red (n=5-8) in tumour tissue. G) Representative photos of CD31-stained tumour sections. Red arrows indicate open blood vessels. Bar graph shows fraction of CD31-positive vessels that were open (n=5-8). Circles in all graphs represent individual mice. Lines and bars in all graphs = mean±s.e.m. Asterisks in all graphs indicate significance (*p≤0.05; panels A, E-G = student t-test; panels C-D = One-way ANOVA). Scale bars (A-D) = 100μm. Scale bars (E-G) = 200μm.

Figure 7: SLC7A11 knockdown or inhibition in human PDAC tumour explants decreased cell proliferation and CAF activation. A) Schematic diagram of explant model and treatment schedule. B-E) Representative photos and quantification (mean+s.e.m.) of (B) αSMA, (C) cytokeratin, (D) Ki67, (E) BrdU staining in human PDAC tumour explants treated with Star 3+indicated siRNA. F-G) Representative photos and quantification (mean+s.e.m.) of (F) αSMA and (G) BrdU staining in human PDAC tumour explants treated with vehicle control or sulfasalazine (SSZ). Quantification of staining in all panels based on Qupath analysis of whole explant sections. Symbols in (A-E) graphs indicate independent human PDAC patients (mean±s.e.m.). Symbols in (F-G) graphs indicate 2 pieces of tissue from same patient. Asterisks indicate significance (*p≤0.05, ** p≤0.01, ***p≤0.001; n=3; student t-test). All scale bars = 50μm.

Downloaded from cancerres.aacrjournals.org on July 31, 2021. © 2021 American Association for Cancer Research.

Author Manuscript Published OnlineFirst on May 12, 2021; DOI: 10.1158/0008-5472.CAN-20-2496
Author manuscripts have been peer reviewed and accepted for publication but have not yet been edited.

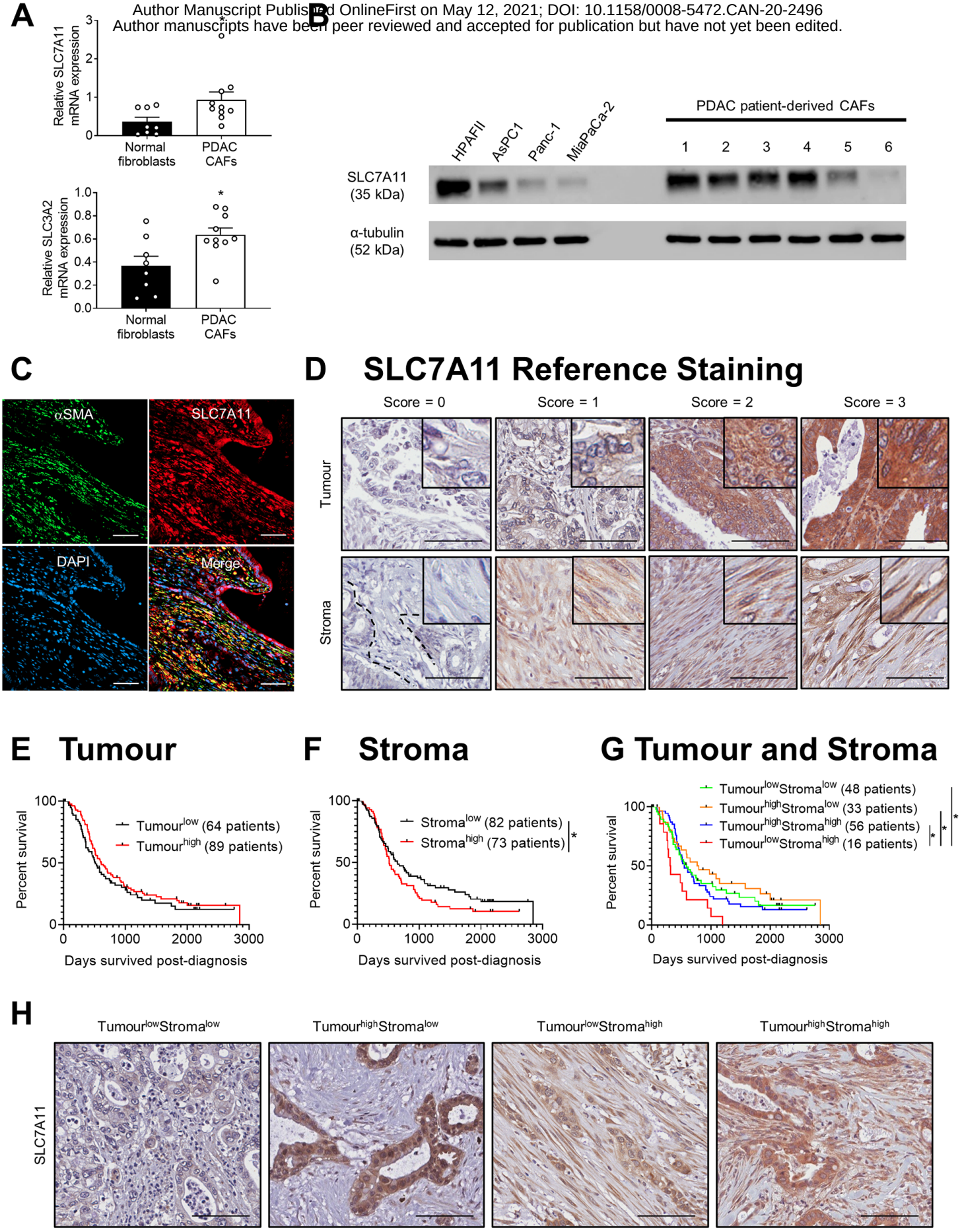


Figure 1

Downloaded from cancerres.aacrjournals.org on July 31, 2021. © 2021 American Association for Cancer Research.

Author Manuscript Published OnlineFirst on May 12, 2021; DOI: 10.1158/0008-5472.CAN-20-2496
Author manuscripts have been peer reviewed and accepted for publication but have not yet been edited.

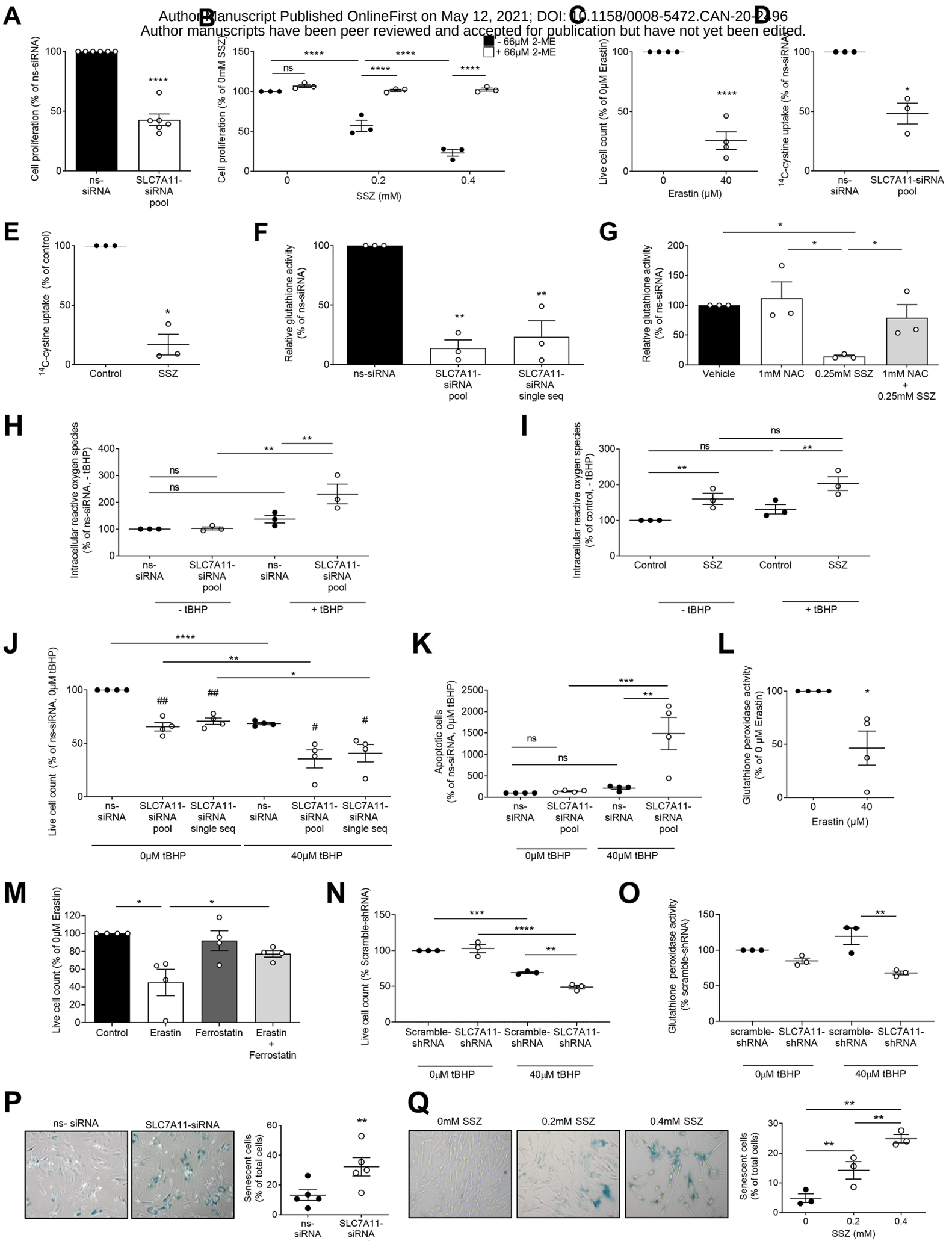


Figure 2

Downloaded from cancerres.aacrjournals.org on July 31, 2021. © 2021 American Association for Cancer Research.

Author Manuscript Published OnlineFirst on May 12, 2021; DOI: 10.1158/0008-5472.CAN-20-2496
Author manuscripts have been peer reviewed and accepted for publication but have not yet been edited.

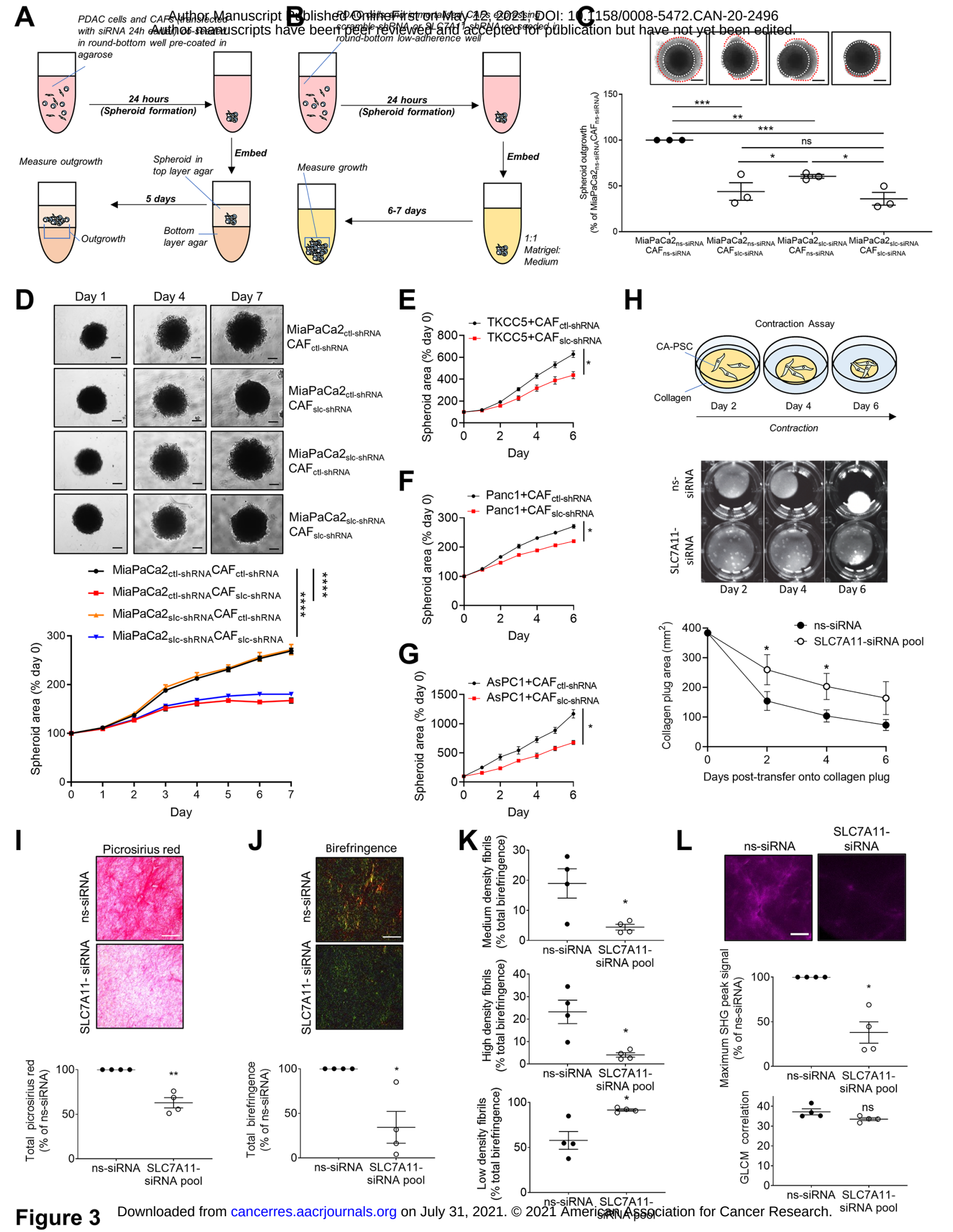


Figure 3

Downloaded from cancerres.aacrjournals.org on July 31, 2021. © 2021 American Association for Cancer Research.

Author Manuscript Published OnlineFirst on May 12, 2021; DOI: 10.1158/0008-5472.CAN-20-2496
Author manuscripts have been peer reviewed and accepted for publication but have not yet been edited.

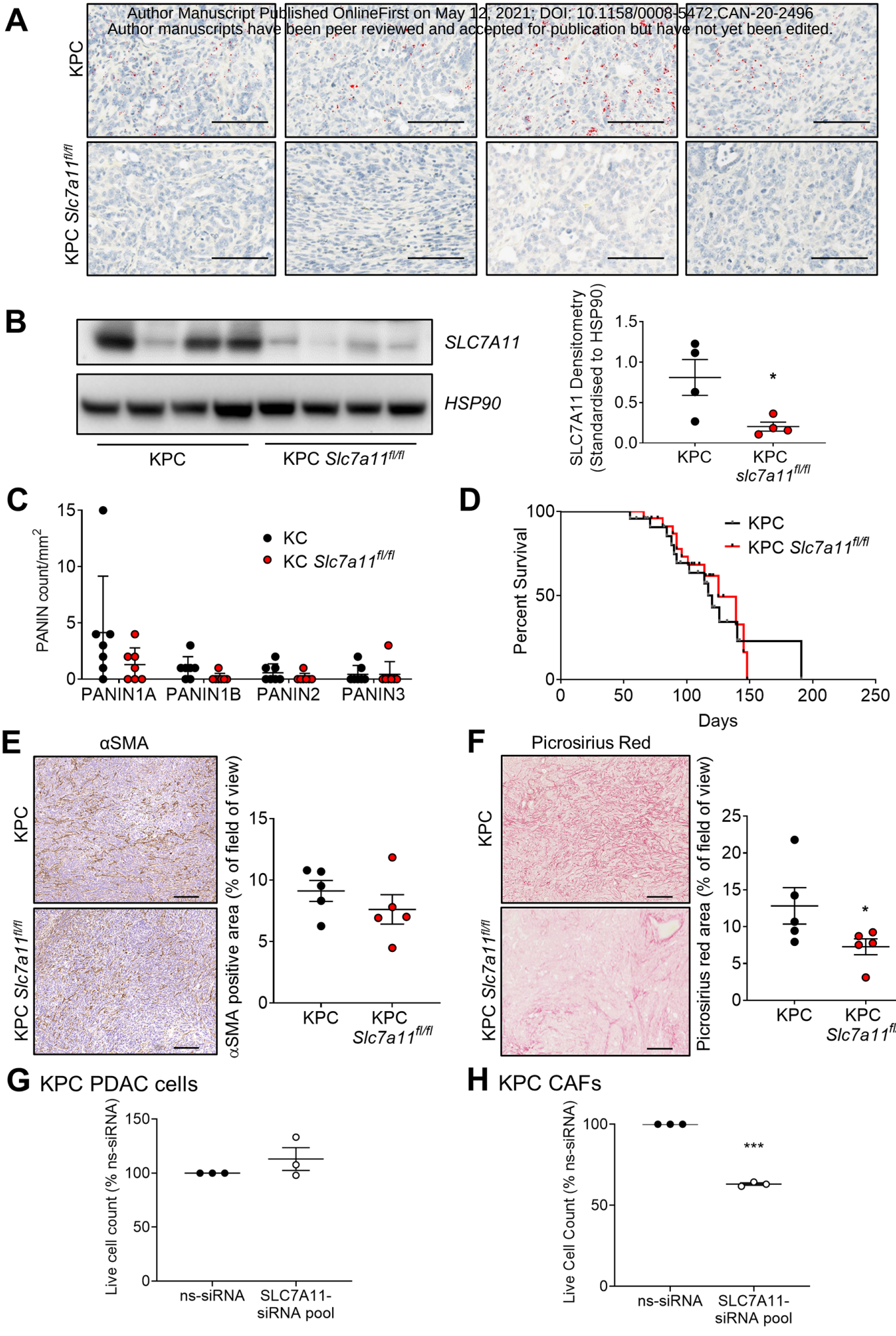


Figure 4

Downloaded from cancerres.aacrjournals.org on July 31, 2021. © 2021 American Association for Cancer Research.

Author Manuscript Published OnlineFirst on May 13, 2021; DOI: 10.1158/0008-5472.CAN-20-2496
Author manuscripts have been peer reviewed and accepted for publication but have not yet been edited.

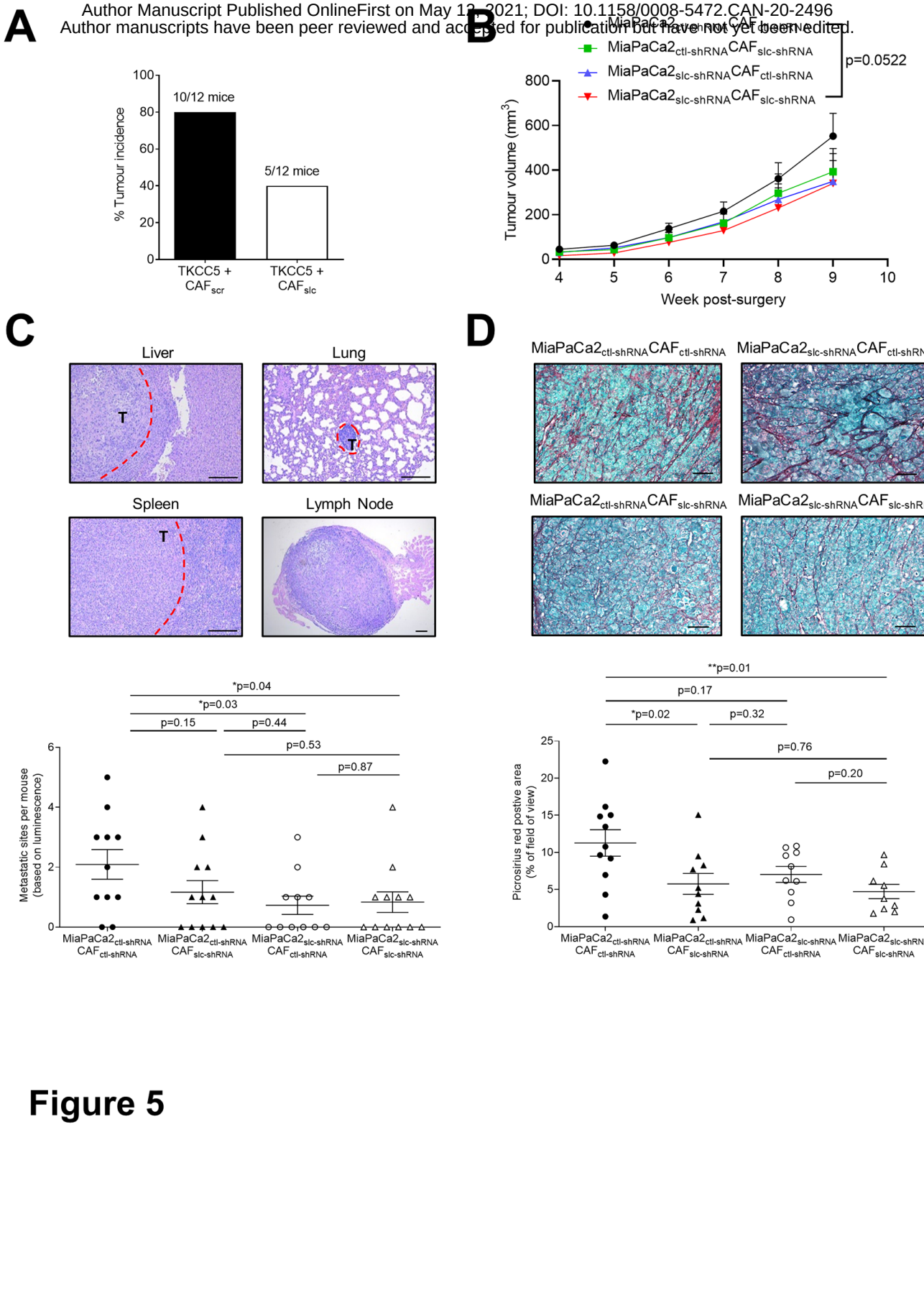
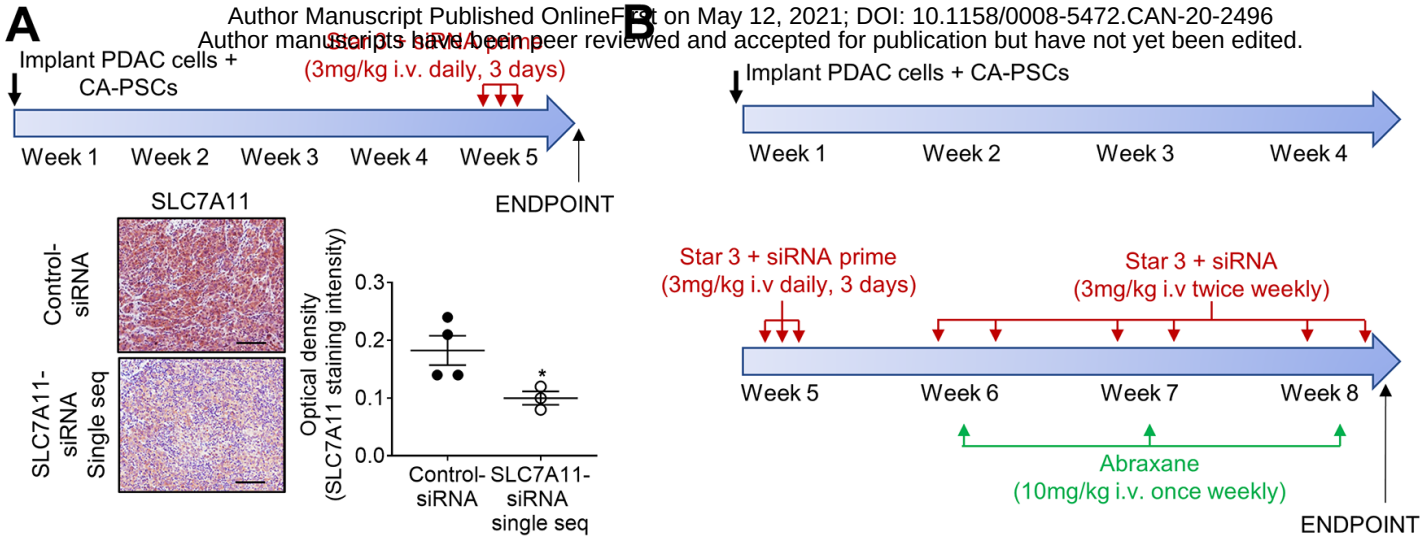
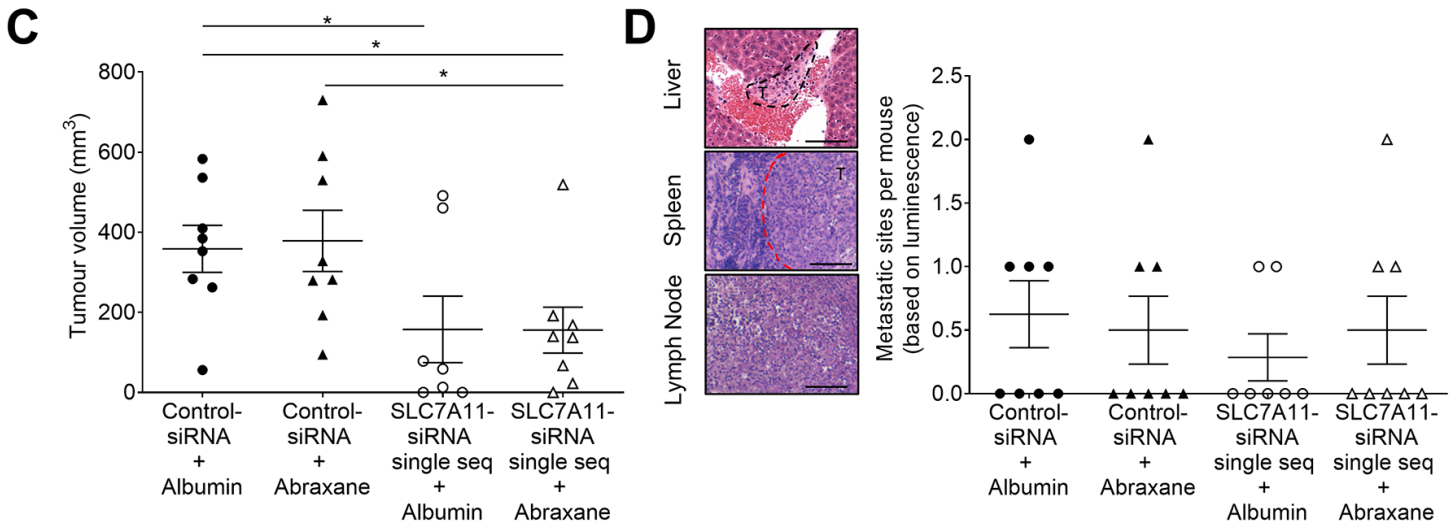


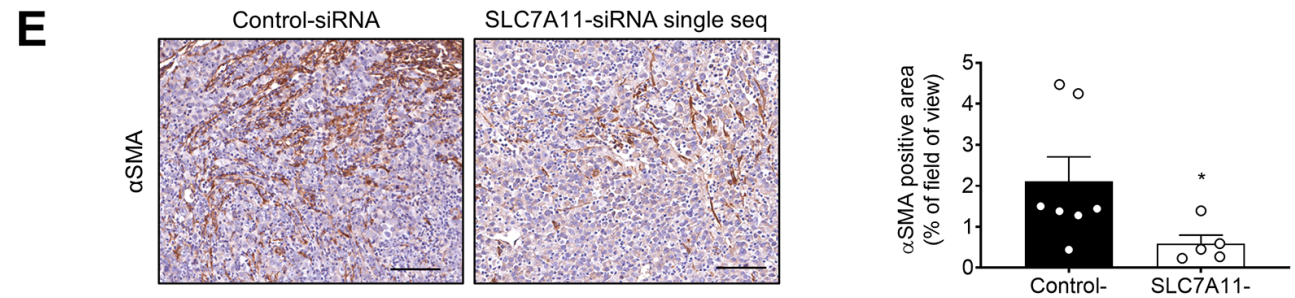
Figure 5

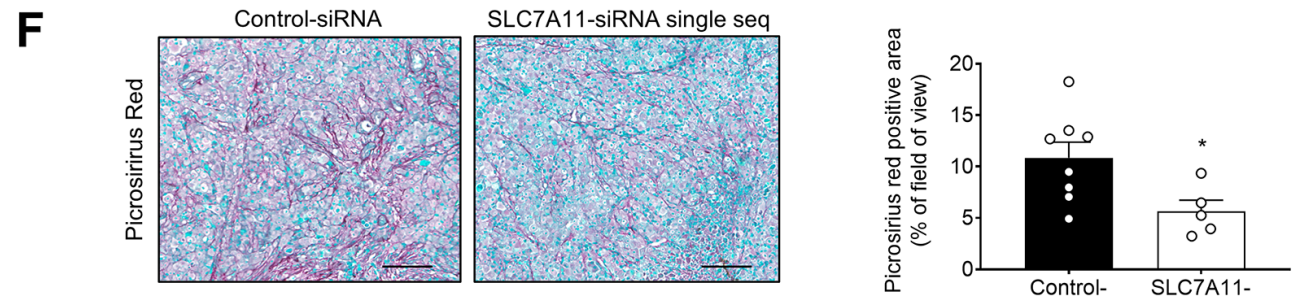
Downloaded from cancerres.aacrjournals.org on July 31, 2021. © 2021 American Association for Cancer Research.

Author Manuscript Published OnlineFirst on May 12, 2021; DOI: 10.1158/0008-5472.CAN-20-2496
Author manuscripts have been peer reviewed and accepted for publication but have not yet been edited.









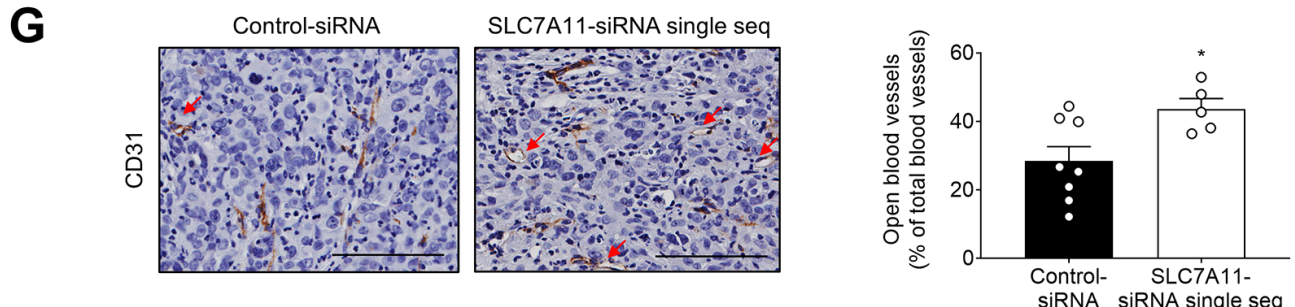
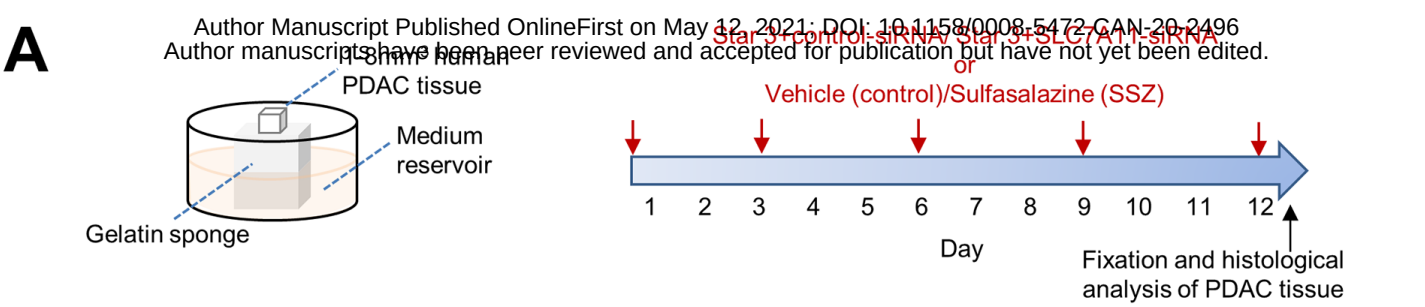
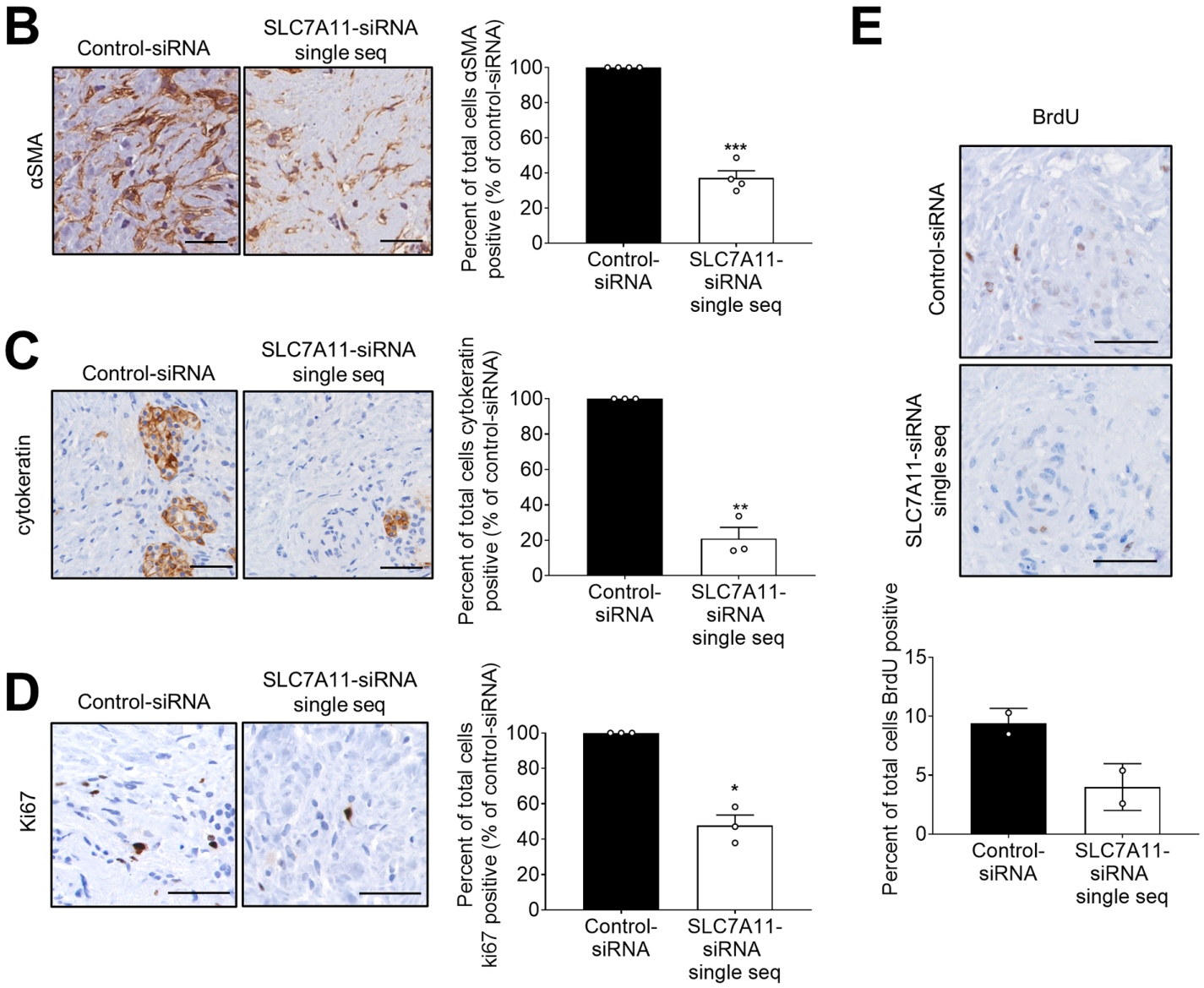


Figure 6

Downloaded from cancerres.aacrjournals.org on July 31, 2021. © 2021 American Association for Cancer Research.

Author Manuscript Published OnlineFirst on May 12, 2021; DOI: 10.1158/0008-5472-CAN-20-2496
Author manuscripts have been peer reviewed and accepted for publication but have not yet been edited.





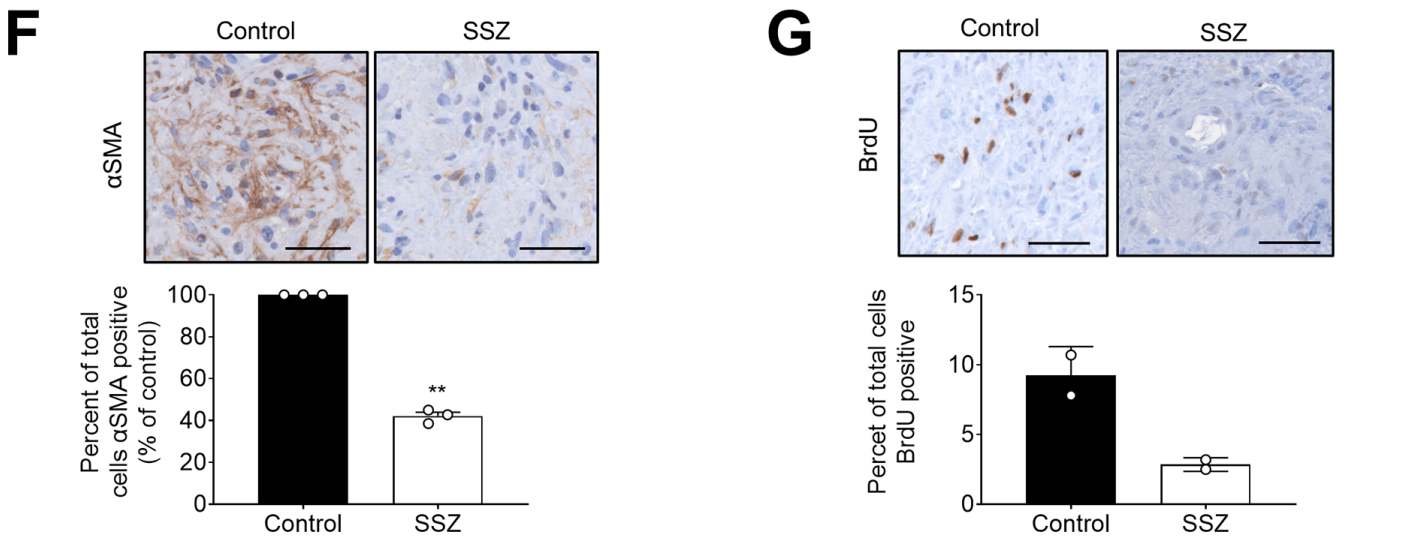


Figure 7

Downloaded from cancerres.aacrjournals.org on July 31, 2021. © 2021 American Association for Cancer Research.

Author Manuscript Published OnlineFirst on May 12, 2021; DOI: 10.1158/0008-5472.CAN-20-2496
Author manuscripts have been peer reviewed and accepted for publication but have not yet been edited.

Cancer Research
The Journal of Cancer Research (1916–1930) | The American Journal of Cancer (1931–1940)

AACR American Association for Cancer Research

Cancer-associated fibroblasts in pancreatic ductal adenocarcinoma determine response to SLC7A11 inhibition

George Sharbeen, Joshua A McCarroll, Anouschka Akerman, et al.

Cancer Res Published OnlineFirst May 12, 2021.

Updated version	Access the most recent version of this article at: doi:10.1158/0008-5472.CAN-20-2496
Supplementary Material	Access the most recent supplemental material at: http://cancerres.aacrjournals.org/content/suppl/2021/04/30/0008-5472.CAN-20-2496.DC1
Author Manuscript	Author manuscripts have been peer reviewed and accepted for publication but have not yet been edited.

E-mail alerts	Sign up to receive free email-alerts related to this article or journal.
Reprints and Subscriptions	To order reprints of this article or to subscribe to the journal, contact the AACR Publications Department at pubs@aacr.org.
Permissions	To request permission to re-use all or part of this article, use this link http://cancerres.aacrjournals.org/content/early/2021/05/07/0008-5472.CAN-20-2496. Click on "Request Permissions" which will take you to the Copyright Clearance Center's (CCC) Rightslink site.

Downloaded from cancerres.aacrjournals.org on July 31, 2021. © 2021 American Association for Cancer Research.